Optimization of synthetically versatile pyridylideneamide ligands for efficient iridium-catalyzed water oxidation

Miquel Navarro,[a] Christene A. Smith,[a,b] Mo Li,[c] Stefan Bernhard,*[c] Martin Albrecht*[a]

[a] Department of Chemistry & Biochemistry, University of Bern, Freiestrasse 3, CH–3012 Bern, Switzerland.

[b] permanent address: Department of Chemistry, Queen's University, 90 Bader Lane, Kingston, Ontario, Canada.

[c] Department of Chemistry, Carnegie Mellon University, 4400 Fifth Avenue, Pittsburgh, PA 15213, USA

E-mail: martin.albrecht@dcb.unibe.ch; bern@cmu.edu

Abstract

The synthetic versatility of PYA ligands has been exploited to prepare and evaluate a diverging series of iridium complexes containing *C,N*-bidentate chelating aryl-PYA ligands for water oxidation catalysis. The phenyl-PYA lead structure **1** was modified (i) electronically through introduction of one, two, or three electron-donating methoxy substituents on the aryl ring, (ii) by incorporating long aliphatic chains to the pyridyl fragment of the PYA unit, and (iii) by altering the PYA positions from *para*-PYA to its *ortho*- and *meta*-isomers. Electrochemistry indicated no substantial electronic effect of the aliphatic chains, and only minor changes of the electron density at iridium when modifying the aryl ligand site, yet substantial alteration if the PYA ligand is the *ortho*- ($E_{1/2}$ = +0.72 V), *para*- ($E_{1/2}$ = +0.64 V) or *meta*-isomer ($E_{1/2}$ = +0.56 V vs SCE). In water oxidation catalysis, the long alkyl chains did not induce any rate enhancement compared to the phenyl-PYA lead compound, while MeO groups incorporated in the aryl group enhanced catalytic activity from a TOF_{max} =1600 h^{-1} in the original Ph-PYA system gradually as more MeO groups were introduced up to a TOF_{max} = 3300 h^{-1} for a tris(MeO)-substituted aryl-PYA system. The variation of the PYA substitution had only a minor impact on catalytic activity and revealed only a weak trend in the sequence *ortho > meta > para*. The high activity of the tris(MeO) system and the ortho-PYA isomer were attributed to efficient hydrogen bonding that assists O–H bond activation and proton transfer. Remarkably merging of the two optimized motifs, i.e. an aryl unit with three OMe substituents and the PYA as *ortho* isomer, into a single new aryl-PYA ligand system failed to improve catalytic activity. Computational analysis suggests too much congestion at the active site, which hinders catalytic turnover. These results illustrate the complexity of ligand design and the subtle effects at play in water oxidation catalysis.

Keywords: ligand design --- N-donor ligands --- mesoionic ligands --- iridium --- water oxidation catalysis

Introduction

Artificial photosynthesis entailing catalytic water splitting is one of the most promising processes to harness and store solar and other renewable energy.[1,2] In pursuit of developing efficient water splitting systems, the water oxidation half-cycle has been demonstrated to be a severe limitation. Hurdles include, *inter alia*, the highly uphill thermodynamics of water oxidation, and as well as the complexity and kinetic barriers associated with the transfer of four protons and four electrons that is required for the formation of O_2.[3] In order to mediate the multiple transfer of electrons and to overcome the energetic barrier of O–H bond cleavage and O–O bond formation, a high redox-flexibility of the catalytic metal center is required.[4] Initial approaches have been inspired by the natural oxygen evolving complex,[5] focusing on di- and tetrametallic systems for chemically driven molecular water oxidation.[6,7] More recently, one of us demonstrated that a single iridium center is active in water oxidation when bound to two phenylpyridyl ligands (**A**, Figure 1).[8] While this work triggered investigations towards single site metal catalysts with other transition metals,[9] including first row transition metal systems,[10] the activity of iridium complexes remained a benchmark.[11,12] The use of stronger donor ligands like Cp* ($C_5Me_5^-$) further enhanced catalytic activity (**B**),[13] and even though strong support is available for a gradual oxidation of the Cp* unit under catalytic conditions,[14] the [Ir(Cp*)] has emerged as a privileged synthon for designing water oxidation catalysts.[11] In particular the introduction of chelating spectator ligands based on strong σ-donors like N-heterocyclic carbenes (NHCs) led to robust molecular catalysts with high activity (**C**).[15,16] Recently, we have introduced pyridylideneamides (PYAs) as strong donor ligands[17] to the [Ir(Cp*)] iridium complex **1** (Figure 1).[18] This complex shows excellent performance in water oxidation catalysis, providing maximum turnover frequencies (TOF_{max}) of 1,600 h^{-1} and up to 86,000 turnovers. This high activity might be attributed to the considerable donor flexibility of the PYA ligand, and the ensuing stabilization of different metal oxidation states during the catalytic process (*cf* limiting resonance structures A and B for **1** in Figure 1).

Here we have capitalized on the synthetic versatility of the phenyl-PYA ligand to optimize the lead iridium catalyst further. Based on recent studies, which showed a substantial rate enhancement by simple alterations on key positions of the ligands,[19,20] we have exploited such modifications for enhancing the catalytic activity of complex **1** by modulating specifically *i*) the donor properties of the Ph ligand, *ii*) the N-substituent on the PYA ligand, and *iii*) the donor properties of the PYA ligand.
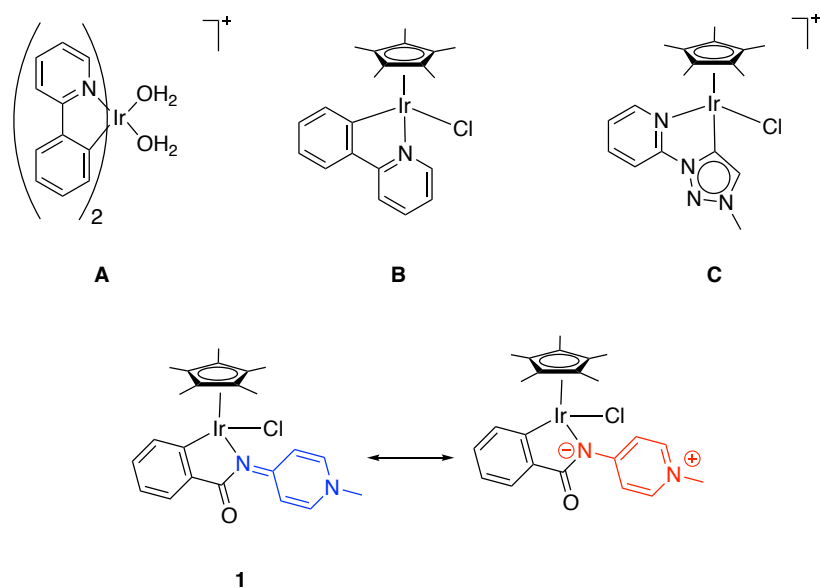
Figure 1. Iridium catalysts for water oxidation catalysis and limiting resonance structures of iridium PYA complex **1**.

Results and discussion

Synthesis of complexes. *i) Variation of donor properties of the Ph unit:* We have recently described synthetic protocols for the introduction of methoxy groups on the phenyl ring of the parent complex **1**.[18] The preparation of these ligands was conveniently achieved due to the availability of the corresponding methoxy-substituted benzoic acids, which were readily transformed to the PYA ligands by reaction with 4-aminopyridine, pyridine alkylation and amide deprotonation. Metalation with [Ir(Cp*)Cl$_2$]$_2$ afforded the cyclometalated complexes **2–5** (Figure 2), which exhibited enhanced catalytic activity in transfer hydrogenation of ketones and imines, as well as in alkyne hydrosilylation.[19] The better catalytic performance relative to complex **1** was attributed to the higher electron density at the active site and the ensuing stabilization of higher oxidation states during the catalytic cycle. In an effort to quantify electronic impact of the different aryl-PYA ligands, we have now performed electrochemical analysis. Cyclic voltammetry (CV) in CH$_2$Cl$_2$ solution revealed a fully reversible oxidation wave that was assigned to an Ir$^{III/IV}$ oxidation process (Figure S1). For complex **1** without any substituent at the phenyl unit, this oxidation is centered at $E_{1/2}$ = +0.64 V *vs* SCE (SCE = saturated calomel electrode), while methoxy-substituents shift the oxidation to lower potential, as expected for electron-donating groups. The half-wave potentials were shifted non-linearly to $E_{1/2}$ = +0.61 V and +0.62 V for **2** and **3**, respectively (both with one MeO group), and to lower potential, $E_{1/2}$ = +0.58 V for complex **4** with two MeO substituents. However, complex **5** with

three MeO units was oxidized at higher potential, $E_{1/2}$ = +0.61 V. While this data helps to rationalize the lower performance of complex **1** in transfer hydrogenation, it is remarkable that the substituent effect is not additive. The lowest oxidation potential was measured for complex **4** with two MeO groups, which was also the most active transfer hydrogenation catalyst. In contrast, a third MeO group in complex **5** increases the potential again slightly, yet the catalytic activity is radically changed and the complex is essentially inactive. The small differences between the oxidation potentials of all complexes **1–5** suggests another limiting effect to reach the +IV oxidation state of the iridium center, especially once the first methoxy substituent is introduced, such as enhanced inductive effects of the oxo substituents, or steric factors imparted by the MeO substituents.
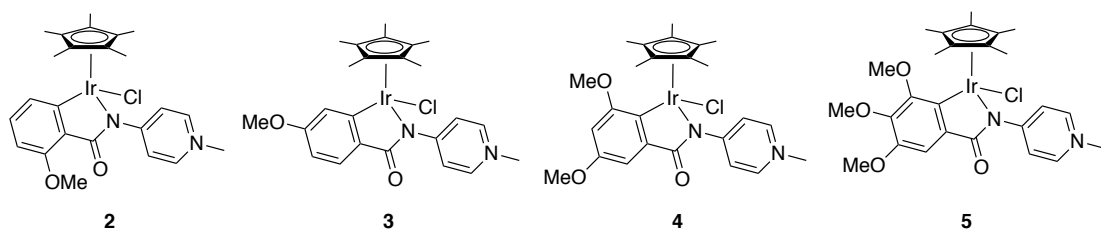

Figure 2. Iridium complexes **2–5** bearing methoxy-substituted PYA ligands.

ii) Modulating the N-substituent on the PYA ligand: Variation of the N-substituent on the PYA unit was motivated by work using triazolylidene iridium complexes for water oxidation.[20] In that work, a ten-fold rate enhancement was observed when substituting a methyl substituent at the triazolylidene heterocycle by an octyl group, which was tentatively attributed to a specific aggregation processes induced by the long aliphatic chain. Based on these data, the pyridyl-bound methyl group of the PYA ligand in complex **1** was substituted with alkyl groups of different length. To this end, *N*-(pyridin-4-yl)benzamide was alkylated with 2-iodopropane, 1-iodobutane and 1-iodooctane to yield the corresponding pyridinium salts **6a–c** in excellent yields (91–95%, Scheme 1). Selective alkylation was unambiguously confirmed by HR-MS analysis, which displayed the expected [M–I]$^+$ mass ion for the isopropyl, butyl and octyl salts at 241.1329, 255.1489 and 311.2111 amu, respectively (theoretical values 241.1341, 255.1492 and 311.2118 amu, respectively) and by ^{1}H NMR spectroscopy, which showed the appearance of a new set of resonances corresponding to the new NC*H* at δ_H = 4.88 (**6a**), and for the NC*H*$_2$ unit at δ_H = 4.47 (**6b**) and 4.44 (**6c**), together with the expected resonances in the aliphatic region of the spectrum. The reaction of **6a–c** with aqueous NaOH afforded the free ligands **7a–c** in good yields (73–84%). The ^{1}H NMR spectra of the free pyridylidene amides

indicated the disappearance of the amide proton around 8 ppm, as well as a significant upfield shift of almost a full ppm for the heterocyclic proton resonances, which is in agreement with previous studies and the relevance of the diene-type resonance structure.[21] In contrast, the aryl proton signals were barely affected, indicating that only the pyridylidene system is involved in stabilizing the deprotonated amide, but not the aryl unit.
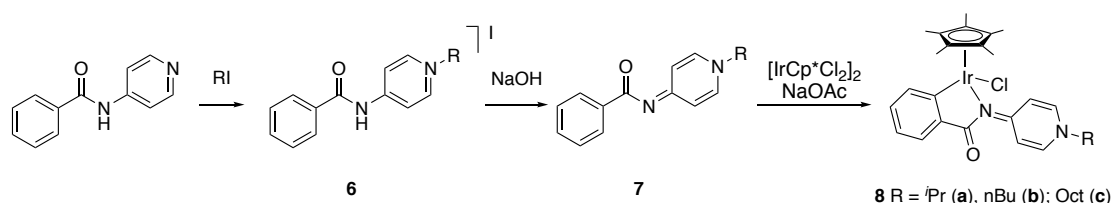
Scheme 1. Synthesis of IrCp*PYA-type complexes **8a–c** with different alkyl chains.

Metalation was performed by reacting the free ligand with [Ir(Cp*)Cl$_2$]$_2$ in the presence of NaOAc as base,[22] which induced cyclometalation and afforded the iridium complexes **8a–c** in good yields (54–75%; Scheme 1). These complexes are air-stable and were purified by standard silica column chromatography without any precaution. Cyclometalation was demonstrated for all the complexes by the loss of one proton signal in the aromatic region of the ^{1}H NMR spectrum. The structures of complex **8b** and **8c** were unequivocally confirmed by single crystal X-ray diffraction analysis (Figure 3). The molecular structures are unsurprising and bond lengths and angles around the iridium center are identical within standard deviations for both complexes and similar to related complexes (Table 1).[19] The pyridyl C$_\alpha$–C$_\beta$ bonds are consistently shorter (average 1.35 Å) compared to the C$_\beta$–C$_\gamma$ bonds (1.41 Å), confirming substantial contribution of the neutral diene-type resonance structure in the solid state, in agreement with previous studies (see Table S1).[19,20,23]
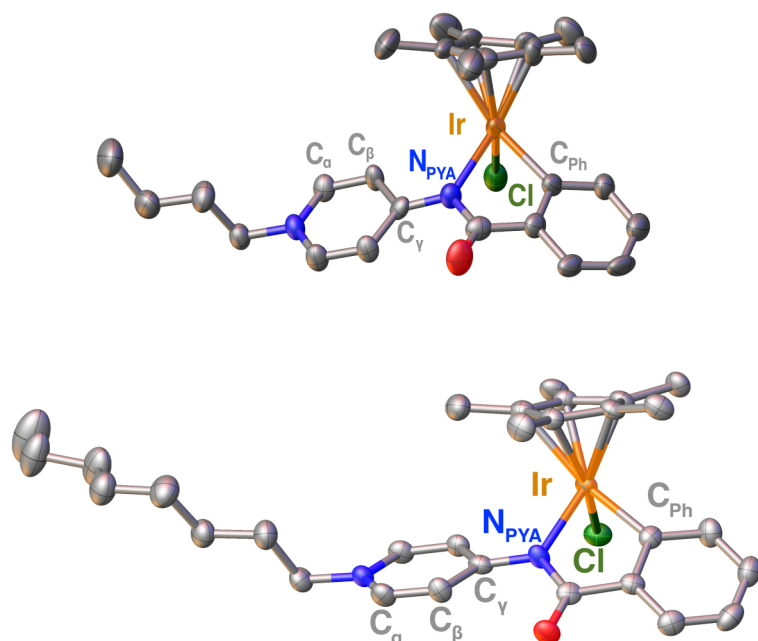
Figure 3. ORTEP diagram of **8b** and **8c**. (50% probability; hydrogen atoms and co-crystallised solvent molecules omitted for clarity, only one of the two independent molecules of **8b,c** in the unit cell shown). Selected bond lengths (Å) and angles (°) for **8b**: Ir–C_{Ph} 2.008(11), Ir–N_{PYA} 2.127(9), Ir–Cl 2.409(3), Ir–Cp(centroid) 1.823(5), C_{Ph}–Ir–N_{PYA} 77.4(4); dihedral angle C(O)–N_{PYA}–C_γ–C_β 24.5(11); for **8c**: Ir–C_{Ph} 2.040(5), Ir–N_{PYA} 2.121(4), Ir–Cl 2.4161(14), Ir–Cp(centroid) 1.820(2), C_{Ph}–Ir–N_{PYA} 77.5(2); dihedral angle C(O)–N_{PYA}–C_γ–C_β 29.1(8).

Electrochemical analysis of complexes **8a–c** by CV in CH_2Cl_2 revealed a fully reversible oxidation at $E_{1/2}$ = +0.64 V *vs* SCE for all complexes **8a–c**, which is identical to the potential measured for complex **1**. This identical oxidation potential indicates that modulation of the N-bound alkyl group has no significant influence on the donor properties of the PYA ligand, nor on the electronic configuration at the iridium center.

iii) Modulation of the PYA donor properties: Modification of the donor properties of the PYA unit was anticipated to be effective by changing the position of the amide unit. While complex **1** may be considered as a *para*-PYA unit with the amide in *para* position of the pyridyl nitrogen, derivatives with the amide in *meta* or *ortho* substitution will have considerably different electronic properties. An *ortho*-PYA system will feature a neutral limiting resonance structure,[24] though the proximity of the N-methyl group and the amide C=O unit is expected to induce a dihedral strain (Scheme 2A). In contrast, the *meta*-PYA unit lacks a neutral resonance form and therefore represents a unique mesoionic *N*-donor system (Scheme 2B), as detailed in a previous communication.[25] Based on these considerations, variation of the substitution pattern was expected to have a pronounced effect on the donor properties.
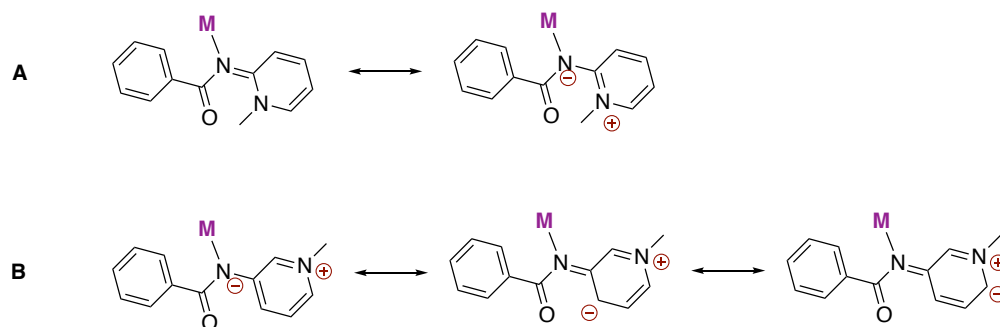
Scheme 2. Limiting resonance structures of a generic *ortho* PYA complex (A, note also the steric constraint of the N–CH₃ group with either the C=O or the ligands at the metal); and some of the relevant resonance structures of a generic *meta* PYA complex (B).

The synthesis of the iridium complexes analogous to **1** but with *meta*- and *ortho*-PYA units was straightforward and started from benzoyl chloride, which was coupled with 2- or 3-aminopyridine to form the amides **9a** and **9b**, respectively (Scheme 3).[26] Subsequent methylation using MeI formed the *meta* pyridinium **10b** in excellent yield (95%), while **10a** was obtained only in a moderate 39% yield. This fact might be due to the lower nucleophilicity of the pyridine nitrogen or because of entropic effects associated with steric rigidity. Both salts showed the characteristic $[M–I]^+$ ion in the HR-MS at 539.1684 and 539.1665 (theoretical value 539.1669 amu). Alkylation was also supported by ¹H NMR spectroscopy, in particular by the appearance of a new singlet for the N–CH₃ group (4.29 and 4.41 ppm for **10a** and **10b**, respectively) as well as a downfield shift of the pyridinium proton signals when compared to the resonances of the pyridine precursors. Due to the lack of symmetry in the heterocycle, both pyridinium systems feature four distinct CH groups both in the ¹H and ¹³C NMR spectra. Amide deprotonation was accomplished with NaOH and afforded the free ligands **11a,b** as yellowish oils in good yields (~70%). The ¹H NMR spectra of the free bases revealed the same characteristic signals as those described for the *para*-PYA **7**, *viz.* disappearance of the amide proton as well as a 0.3–1.1 ppm upfield shift of the resonance frequencies of the heterocyclic protons.[21]

The reaction of the free ligands with [Ir(Cp*)Cl₂]₂ in the presence of NaOAc induced cyclometalation and yielded, after purification by column chromatography, the iridium complexes **12a** and **12b** in good yields (~70%) as orange air-stable solids (Scheme 2). ¹H NMR spectroscopy confirmed cyclometalation for both complexes by the loss of one proton signal in the aromatic region. Four distinct signals were present each for the pyridylidene unit as well as for the cyclometalated aryl ring.
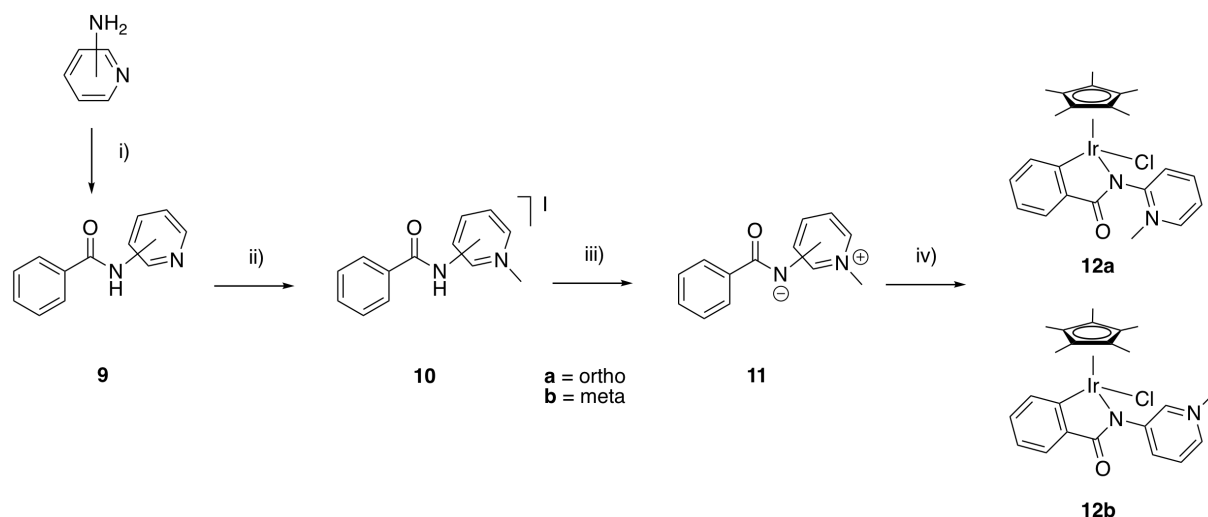
Scheme 3. Synthesis of iridium complexes **12a** and **12b**. i) PhCOCl, NEt$_3$; ii) MeI; iii) NaOH; iv) [Ir(Cp*)Cl$_2$]$_2$, NaOAc.

The molecular structure of complex **12b** with a mesoionic PYA ligand was further investigated by single crystal X-ray diffraction analysis. The complex reveals the classical three-legged piano-stool geometry with a pseudo-tetrahedral iridium center (Figure 4). Bond lengths and angles around the iridium center are similar to those of the related iridium complexes **1–5**,[18,19] and **8** (*vide supra*). However, the C–C and N–C bonds of the pyridylidene unit do not show any bond length alteration pattern, supporting the low relevance of a diene-type structure with localized double bonds as noted for the *para*-PYA free ligands and complexes **1–5**. All C–C bond length distances are equivalent within standard deviation and indicate high double bond conjugation as expected for an aromatic pyridyl ring.
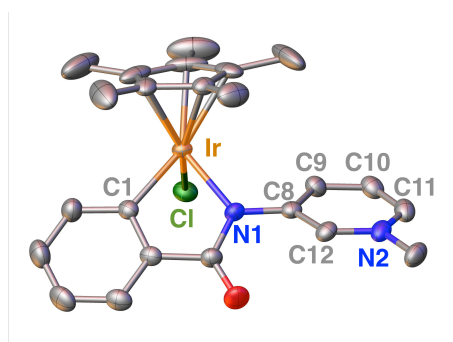
Figure 4. ORTEP diagram of iridium complex **12b** (thermal ellipsoids at the 50% probability level; hydrogen atoms, co-crystallized solvent molecules, and second independent molecule of the unit cell omitted for clarity). Selected bond lengths (Å): Ir–C1 2.035(3), Ir–N1 2.103(2), Ir–Cl 2.4219(8), Ir–Cp(centroid) 1.819(2), C8–C9 1.399(4), C8–C12 1.401(4), C9–C10 1.385(4), C10–C11 1.381(5). Selected bond angles (deg): C1–Ir–N1 77.83(11), C1–Ir–Cl 86.42(8), N1–Ir–Cl 87.89(7); dihedral angle C(O)–N1–C8–C9 39.0(3).

The donor properties were evaluated by electrochemical analysis. CV in CH_2Cl_2 revealed a fully reversible oxidation process at $E_{1/2}$ = +0.72 (*vs* SCE) for the *ortho*-PYA complex **12a** and at +0.56 V (*vs* SCE) for complex **12b** with a *meta*-PYA ligand (Figure 5). These potentials diverge considerably from the +0.64 V measured for the parent *para*-PYA complex **1** and indicate that the mesoionic PYA ligand **11b** is a substantially stronger donor than *para*-PYA. Such stronger donor ability is expected when considering that π-acidic imine-type bonding of the PYA ligand is disfavored in the mesoionic *meta*-PYA ligand, but much less in the *para*-PYA isomer. The significantly higher oxidation potential of complex **12a** is remarkable and suggests that the *ortho*-PYA ligand is much less suitable for stabilizing higher metal oxidation states. The 80 mV potential difference between the *para*- and *ortho*-PYA is substantial, and presumably does not originate from simple resonance structure effects, but may relate to out of plane distortion of the PYA ligand instead.
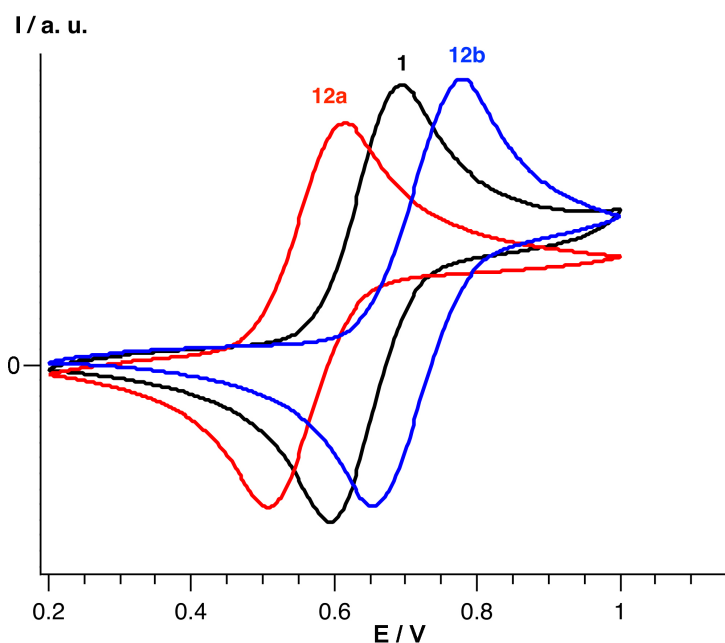

Figure 5. Superimposed CV plots of complexes **1** (black), **12a** (blue) and **12b** (red) in CH_2Cl_2 solution (0.1 M Bu_4NPF_6 as supporting electrolyte, 100 mV s^{-1} scan rate, potential *vs* SCE.

Catalytic water oxidation. The structurally modified iridium complexes **2–5**, **8a,b,c**, and **12a,b** as well as the non-substituted parent complex **1** were investigated for catalytic water oxidation. The processes were chemically driven by $(NH_4)_2[Ce(NO_3)_6]$ (CAN), a one-electron oxidant unable to oxidize water without a catalyst (Figure 6). All Ir(III) complexes were soluble in water (solubility at least 1 mg mL^{-1}), and in the presence of CAN dissolved with 1M HNO_3, immediate gas formation was observed and quantified dynamically with the homebuilt pressure

transducer setup.[8] Complexes **8b** and **8c** have limited solubility in water due to the attached long alkyl chains (*n*Bu and Oct respectively), and thus their concentrations used in the water oxidation experiments did not exceed 20 μM, while all the other complexes were tested at concentrations up to 50 μM. Stability tests in 0.1 M HNO_3 (pH 2), and in the presence of 4 molequiv. CAN did not indicate any complex degradation, nor loss of the MeO substituents (Fig. S2).[27] Quantitative analysis of the oxygen evolution revealed higher or equivalent activity of complexes **2–5, 8**, and **12** in comparison to the parent complex **1** (Table 2, entries 1–5). Methoxy substituents accelerated the catalytic rates: mono-substituted complexes **2** and **3** displayed TOFs of 2400 h^{-1} and 1800 h^{-1} respectively (entries 6–11), while di-substituted complex **4** (entries 12–14) and tri-substituted complex **5** (entries 15–17) proved to be the most active catalysts exhibiting TOFs that exceeded 3000 h^{-1}. As for the transfer hydrogenation catalysis, the incorporation of electron-donating groups enhances the catalytic activity in the water oxidation reaction, an effect that culminated with complexes **4** and **5**, two of the most active iridium catalyst reported to date.[28] These rate differences are considerable, and interestingly they are not correlated with the electrochemical measurements. Obviously higher oxidation states than the +IV species will need to be reached in a catalytic cycle and the electrochemically measured $Ir^{III/IV}$ redox potentials are therefore not correlated to turnover-limiting processes. Though it is worth noting that there is no extrapolation from these potentials to the critical step of the catalytic cycle.[29]
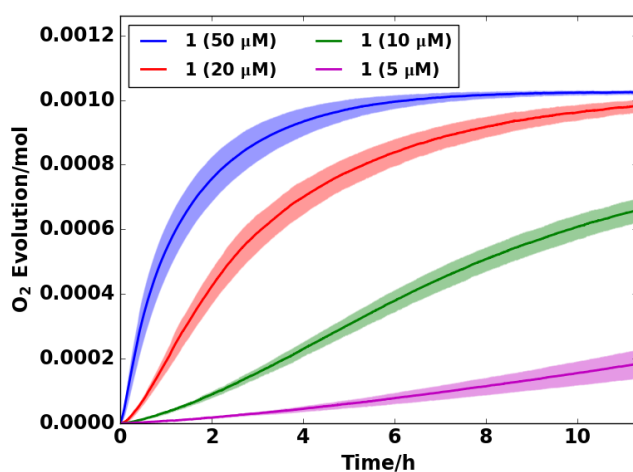

Figure 6. Oxygen evolution traces of the initial 11 h of water oxidation catalyzed by complex **1** at different concentrations (4.5-49.6 μM; for accurate concentrations of the complex, see Table 1). Solid lines represent the average of multiple measurements. Faded areas illustrate error bands at 95 % confidence interval.

Complexes **8a–c** with different alkyl groups attached the pyridyl nitrogen all display about the same TOF as observed with complex **1** (~1500 h^{-1} at ~50 μM and ~1100 h^{-1} at ~20 μM; entries 18–25). These results suggest that self-aggregation—as hypothesized in previous studies[20]—is not a key issue in this catalytic process, and that the presence of long alkyl chains in the triazolylidene system may therefore have different effects.[30]

Table 1. Catalytic water oxidation with complex **1–5, 8a–c** and **12a,b**.[a]

Entry	Complex	conc. [μM]	CAN/complex	TON	TOF$_{max}$ (h^{-1})
1	**1**	49.6	7380	1,880 ± 30	1,600 ± 500
2	**1**	19.9	20200	4,670 ± 90	1,200 ± 200
3	**1**	9.9	40380	9,700 ± 200	840 ± 20
4	**1**	4.5	80580	19,000 ± 1000	560 ± 60
5	**1**	0.9	406510	86,000 ± 1000	160 ± 10
6	**2**	50.1	7300	1,920 ± 30	2,400 ± 500
7	**2**	19.9	18450	4,730 ± 90	1,600 ± 200
8	**2**	4.5	81180	19,000 ± 400	600 ± 100
9	**3**	49.1	7450	1,920 ± 30	1,800 ± 400
10	**3**	19.6	18730	4,900 ± 100	1,400 ± 200
11	**3**	4.5	81180	20,000 ± 400	700 ± 100
12	**4**	49.7	7370	1,870 ± 20	3,300 ± 700
13	**4**	19.8	18520	4,770 ± 50	1,500 ± 200
14	**4**	4.6	79870	19,000 ± 300	700 ± 100
15	**5**	50.1	7300	1,900 ± 30	3,200 ± 700
16	**5**	20.3	18090	4,680 ± 50	1,600 ± 100
17	**5**	4.6	79910	19,000 ± 300	650 ± 90
18	**8a**	50.4	7240	1,840 ± 20	1,500 ± 300
19	**8a**	0.9	406510	79,000 ± 1000	130 ± 10
20	**8b**	19.8	20250	4,910 ± 80	1,100 ± 100
21	**8b**	9.9	40500	10,000 ± 300	900 ± 200
22	**8b**	4.9	80990	17,800 ± 400	500 ± 100
23	**8c**	20.2	19820	5000 ± 90	1,100 ± 100
24	**8c**	10.1	39640	9,600 ± 200	800 ± 100

25	**8c**	5.1	79270	$18{,}200 \pm 400$	540 ± 80
26	**12a**	49.9	7360	$1{,}850 \pm 30$	$1{,}800 \pm 300$
27	**12a**	19.6	18790	$4{,}700 \pm 100$	$1{,}400 \pm 300$
28	**12a**	9.8	37380	$9{,}300 \pm 100$	$1{,}000 \pm 200$
29	**12a**	4.9	74750	$17{,}500 \pm 100$	700 ± 200
30	**12b**	49.9	7360	$1{,}860 \pm 20$	$1{,}700 \pm 400$
31	**12b**	19.6	18790	$4{,}640 \pm 90$	$1{,}300 \pm 200$
32	**12b**	9.8	37380	$9{,}100 \pm 200$	700 ± 300
33	**12b**	4.9	74750	$17{,}400 \pm 400$	500 ± 300

[a]Measurements were performed in a sealed 40 mL EPA vial containing 10 mL 0.4M CAN solution buffered in 1M HNO_3 and the appropriate complex. O_2 evolution was dynamically monitored with digital manometry and end points were calibrated by gas chromatography; TOF_{max} values were determined by calculating the rate of change of the generated oxygen over time from the kinetic trace.

The water oxidation catalytic activity of the regioisomers **12a** and **12b** of the parent *para*-PYA complex **1** was also evaluated (Table 2). Complex **12b** with a mesoionic PYA ligand displayed water oxidation activity similar to that of the 4-substituted complex **1**, reaching TOF of ~1700 h^{-1} (entries 30–33). This activity enhancement is marginal at best, despite the presence of a more electron-donating mesoionic ligand, which was expected to stabilize higher oxidation states better than the *ortho*- and *para*-PYA ligands (*cf* electrochemistry above). Surprisingly, complex **12a** bearing a lower donor strength ligand than analogues **1** and **12b** shows about the same performance as the other two regioisomers and achieves TOFs up to 1800 h^{-1} (entries 26–29). Obviously, catalytic activity is not controlled solely by the donor strength of the ligand, but also by other factors such as steric influences that affect the (de)stabilization of the metal-bound water or hydroxide intermediates during the catalytic reaction.

DFT modeling was used to rationalize the structure-activity relationship observed for these catalysts. A geometry optimization (B3LYP/LANL2DZ) indicated why compounds **4** and **5** were outperforming the other catalysts: the oxygen lone-pair of the methoxy group is in close proximity to the aqua ligand and forms a strong hydrogen bond (Figure 7a). This arrangement facilitates the deprotonation of this aqua site, especially as oxidation of the Ir(III) center increases the acidity of the linked proton dramatically.[16c,31] Such hydrogen bonding and transfer can be repeated for the second proton after the iridium center is further oxidized to the Ir^{IV}–OH species, a process which constitutes a pathway for efficient proton-coupled electron transfer (PCET) and therefore results in a low-energy pathway towards a very reactive oxo-complex.

The PCET processes have been found to accelerate water oxidation in biological systems as well as in artificial electrochemically or chemically driven processes.[32]

The smaller rate increase observed with complexes **12a** and **12b** is less obvious from the DFT structures. A hydrogen bond between the carbonyl group and the methyl group forming the pyridinium moiety stabilizes the ligand and induces a significant dihedral angle between the pyridylidene heterocycle and the phenylamide portion of the ligand ($\theta = 53°$), which weakens the electronic conjugation and lowers the relevance of the diene-type resonance structure (Figure 7b). It is important to note that the increase in reactivity imparted by this twist due to steric crowding is less notable than that caused by the direct link formed by the hydrogen bond between the methoxy group and the aqua ligand in **4** and **5**.
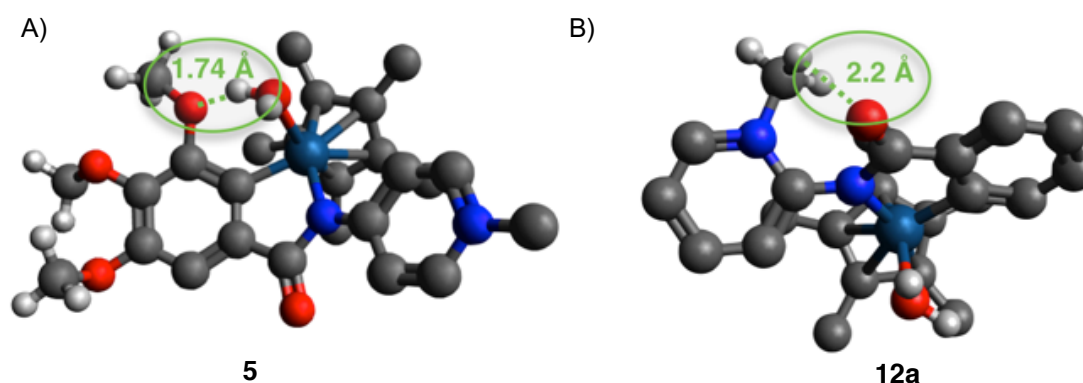

A) 1.74 Å
5

B) 2.2 Å
12a

Figure 7. Hydrogen bonds lead to faster water oxidation: a) The methoxy group attached to the carbon adjacent to the cyclometalating site in complexes **4** and **5** is optimally positioned for accepting the proton from the aquo (and likewise hydroxyl) ligand upon oxidation of the iridium center; b) A weak hydrogen bond between the PYA N–CH$_3$ and the amide CO group stabilizes the *ortho*-PYA ligand in **12a** at a bigger dihedral angle (53°), which increases its donor strength compared to the considerably flatter *para*-substituted parent compound **1**.

Catalyst optimization. While the introduction of long aliphatic chains had no effect on catalyst activity, modulation of the donor properties of both the phenyl group (by introducing electron-donating methoxy substituents) and the PYA residues (by introducing mesoionic *meta*-PYA or sterically constrained *ortho*-PYA motifs) led to more active water oxidation catalysts. Merging these two leading catalyst design strategies was therefore a clear path to further improve the performance of the catalyst. The synthesis and characterization of the mesoionic target complex **16b** has been communicated recently.[25] The analogue featuring an *ortho*-PYA ligand was prepared along the same route starting from the trimethoxy-substituted benzoyl chloride and 2-aminopyridine to form the amide **13**, followed by selective pyridine methylation with MeI to

form the corresponding pyridinium salt **14** (Scheme 4). Deprotonated of the amide with aqueous NaOH afford the free PYA ligand as air-stable solid. The structure of the mesoionic PYA **15b** has been reported as the first example of a mesoionic N-donor ligand.[25] Complexation to iridium and cyclometalation was performed as described above in the presence of NaOAc and yielded the iridium complexes **16a,b** in good yields (69–77%). Both complexes were fully characterized by NMR spectroscopy and HR-MS. In addition, single crystals of iridium complex **16a** were obtained and analyzed by X-ray diffraction (Figure 8). The overall molecular geometry as well as bond lengths and angles around the iridium center are similar to the other structures reported here. Specifically, contribution of the diene-type resonance form of the *ortho*-PYA unit was noted by the bond length alteration in the heterocycle. The C8–C9 and C10–C11 bond lengths are 1.391(5) Å and 1.397(6) Å, respectively, and slightly longer than the C9–C10 and C11–C12 bonds (1.374(5) and 1.353(6) Å, respectively). These differences are smaller than in the *para*-PYA ligand of complexes **1–5**, and **8a–c**, but distinct from the mesoionic and fully conjugated *meta*-PYA system in complex **12b** (*cf* Figure 4). Moreover, the pyridylidene heterocycle is significantly twisted out of the phenylamide plane, as indicated by the C7–N2–C8–N1 torsion angle $\theta = -60.40(4)°$. This value is close to the 53° predicted by DFT for these *ortho*-PYA iridium complexes (*cf* Figure 7b) and hence validate the steric argument suggested for the rate enhancement observed for complex **12a**. Moreover, the distance between the N–CH$_3$ proton and the amide oxygen atom is 2.337(2) Å, very similar to the 2.22 Å predicted by DFT calculations.
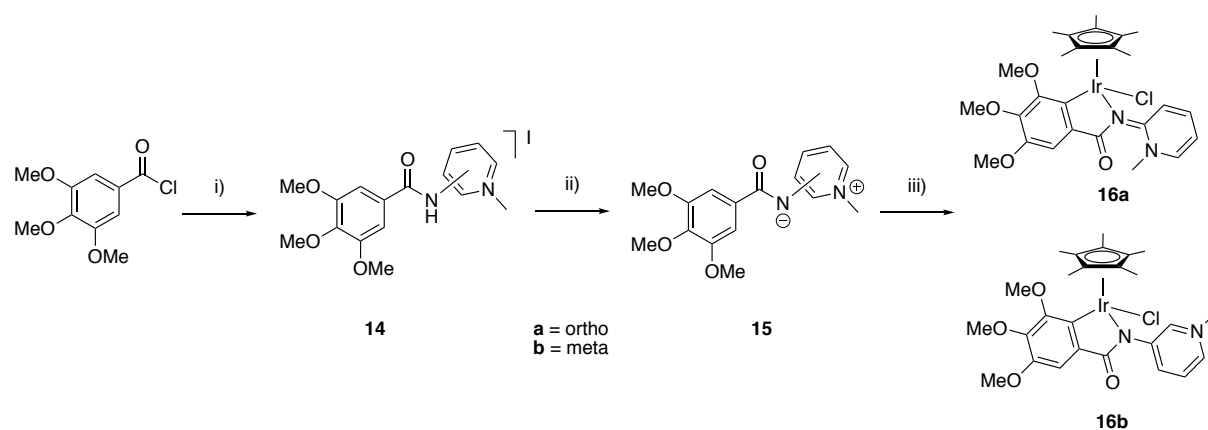
Scheme 4. Synthesis of iridium complexes **16a** and **16b**. i) 2- or 3-aminopyridine, NEt$_3$, MeI. ii) NaOH. iii) [Ir(Cp*)Cl$_2$]$_2$, NaOAc.
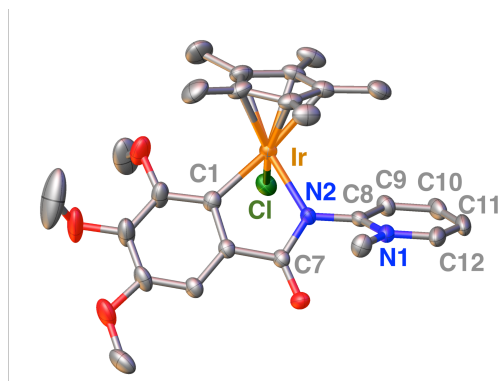
Figure 8. ORTEP diagram of iridium complex **16a**. Thermal ellipsoids are given at the 50% probability level; hydrogen atoms and co-crystallized solvent molecules are omitted for clarity. Selected bond lengths (Å): Ir–C1 2.051(3), Ir–N2 2.116(3), Ir–Cl 2.4274(9), Ir–Cp(centroid) 1.8189(16), C8–C9 1.391(5), C9–C10 1.374(5), C10–C11 1.397(6), C11–C11 1.353(6), N2–C8 1.370(4), C8–N1 1.370(4), C12–N1 1.363(4). Selected bond angles (deg): C1–Ir–N1 77.40(12), C1–Ir–Cl 85.67(8), N2–Ir–Cl 87.33(8). The twisted out of plane distortion of the PYA ligand is clearly visible (dihedral angle C7–N2–C8–N1 60.40(4)°).

Electrochemical analysis (CV) revealed a reversible oxidation potential at $E_{1/2}$ = +0.69 and +0.55 V *vs* SCE for complexes **16a** and **16b**, respectively. The potentials are moderately lower by 30 and 10 mV when compared to the potentials of the corresponding complexes without methoxy substituents ($E_{1/2}$ = +0.72 for complex **12a** and +0.56 V for **12b**). A similar lowering of the oxidation potential by 30 mV was observed upon introduction of three MeO groups in the *para*-PYA complex **1** ($E_{1/2}$ = +0.64 V, *vs* +0.61 V for **5**).[33]

Table 3. Catalytic water oxidation with complex **16a** and **16b**.[a]

Entry	Complex	conc. [µM]	CAN/complex	TON	TOF_{max} (h^{-1})
1	**16a**	49.9	7360	1810±30	1600±400
2	**16a**	19.9	18440	4590±30	1160±80
3	**16b**	49.9	7360	1810±40	1500±400
4	**16b**	19.9	18440	4600±70	1210±60

[a] Measurements were performed in a sealed 40 mL EPA vial containing 10 mL 0.4M CAN solution buffered in 1M HNO_3 and the appropriate complex. O_2 evolution was dynamically monitored with digital manometry and end points were calibrated by gas chromatography; TOF_{max} values were determined by calculating the rate of change of the generated oxygen over time from the kinetic trace.

Even though each of the two structural features employed in the ligand design of complexes **16a** and **16b**, *viz* the three methoxy substituents on the cyclometalating phenyl group (*cf* complex **5**) and the variation of the PYA ligands (*cf* complexes **12a** and **12b**), individually improved water oxidation, the water oxidation activity of complexes **16a** and **16b** is much more aligned with the performance of the parent complex **1**, and no improved performance was

observed (Table 3). The activity of both **16a** and **16b** is less than that of the methoxy-free homologues **12a** and **12b** (*e.g.* for complex **16a**, TOF_{max} at 50 μM catalyst concentration is 1600 h^{-1} *vs* 1800 h^{-1} for **12a**) and substantially lower than that of the $(MeO)_3$-substituted *para*-PYA analogue **5** (TOF_{max} = 3200 h^{-1} under identical conditions). Similarly, complex **16b** reaches a TOF_{max} = 1500 h^{-1} at 50 μM iridium concentration, which is also lower than complex **12b** without methoxy groups (TOF_{max} = 1700 h^{-1}).

Structural analysis of the aqua intermediate by DFT (B3LYP/LANL2DZ) calculations offered two possible explanations for the underperformance of these two complexes, namely lower stability of the complex and lower accessibility of the catalytically active site. First, moving the pyridinium site from the isolated 4-position to the more crowded parts of the molecule increased the steric energy of the complexes significantly. The calculated heat of formation for the *meta*-PYA complex **16b** is 6.2 kcal mol^{-1} higher, while the *ortho*- regioisomer **16a** has a 7.6 kcal mol^{-1} higher energy than the most stable complex **5**. Second, the steric effects observed in the more congested isomers cause substantial twisting of the PYA ligand that is amplified by the three added methoxy groups. While the increase in steric energy might lead to an easier degradation of the two more congested complexes during catalysis, it is also evident that access to the active site is hindered by the twisted pyridinium ring. Figure 9 highlights this effect with a space-filling model of the two regioisomers **5** and **16a** containing a substrate water molecule bound to iridium rather than a chloride. At a certain point on the catalytic cycle, water has to attack the oxygen of the active site to form an O–O bond.[3b] This attack is partially hindered by the congestion and the ensuing twisting of the ligand in complex **16a** (dashed green arrow), and this reduced access will decrease water oxidation rates of this catalyst. In contrast, access to the iridium-bound ligand is much less restricted in complex **5** (solid green arrow).[34]
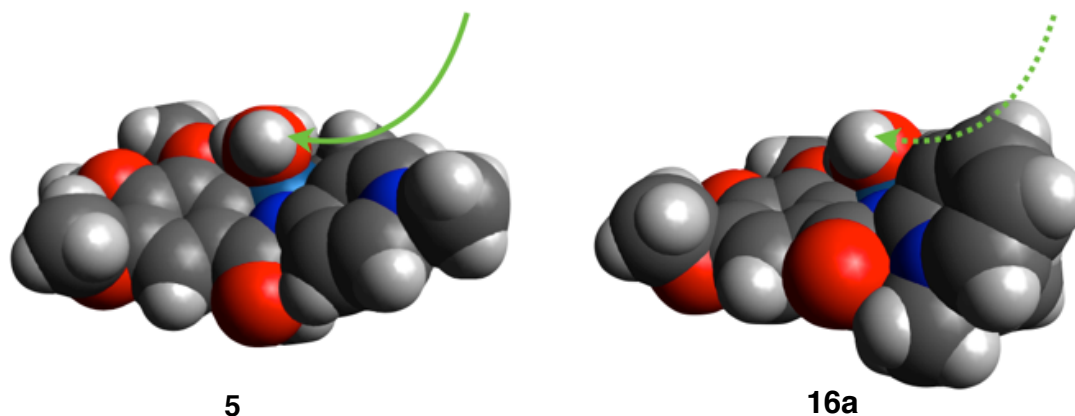

5   **16a**

Figure 9. DFT calculations (B3LYP/LANL2DZ) were used to produce optimized structures of the *para*-PYA complex **5** and the regioisomeric *ortho*-PYA complex **16a**. The access to the active site required to form a O–O

bond is hindered by the twisted pyridinium ring (dashed arrow, arrow head pointing to coordinated water molecule), which leads to a decrease in reaction rates in **16a** and **16b** when compared with the isomeric champion catalyst **5** (compare accessibility of iridium (light blue) and coordinated water molecule as indicated by solid arrow). The increased steric energy of **16a** and **16b** might also lead to a more rapid degradation of these two catalysts.

Conclusions

We have successfully exploited the synthetic versatility of PYA ligands to prepare and evaluate a diverging series of iridium complexes containing chelating aryl-PYA ligands for water oxidation catalysis. Simple modifications, either by incorporating long aliphatic chains, or through electronic modulation by introducing electron-donating methoxy substituents on the aryl ring, or by altering the PYA positions (*ortho-, meta-, para*-PYA), were evaluated to optimize iridium-catalyzed water oxidation. While the incorporation of long alkyl chains had no significant effect, electronic modulation was effective and led to a substantial enhancement of catalytic activity and doubled the catalytic activity of the original lead compound to a TOF_{max} = 3300 h^{-1}. This rate is substantially faster than most of the iridium-based water oxidation catalysts (typically 1000–1800 h^{-1}), but lower than the fastest triazolylidene or pyridyl-carboxylate catalysts (TOF_{max} 7,000–15,000 h^{-1}). Even though optimization of the aryl and the PYA domains of the aryl-PYA chelate each led to improved catalysis, merging of the two optimized motifs in a single new aryl-PYA ligand failed to improve catalytic activity. Computational insights suggest an over-congestion at the active site, which hinders catalytic turnover. Moreover, these results indicate that optimization of the second coordination sphere provides an effective approach for further enhancing the catalytic activity of the metal center, particularly through introduction of advantageous hydrogen bonding sites. These results illustrate the complexity of ligand design and the subtle effects at play in catalytic reactions, and they emphasize the high versatility of the PYA platform for optimizing catalytic activity. Finally, it is worth noting that the electrochemical analysis of the catalyst precursors showed no correlation with catalytic activity. Since the stringent structure-activity relationship observed in this series of complexes is consistent with a molecularly defined catalytically active site, different mechanisms such as redox potentials of the pre-activated species appear to be relevant for facilitating catalytic turnover. Such mechanisms are not necessarily correlated to properties of the catalyst precursor, as demonstrated here with the electrochemical data.

Experimental

General. The metal precursor salt [Ir(Cp*)Cl$_2$]$_2$[35] and complexes **1**,[18] **2–5**,[19] and compounds **9**,[26] **14b–16b**[25] were all synthesized as reported in the literature. All other reagents were commercially available and used as received. Unless specified otherwise, NMR spectra were recorded at 25 °C on Bruker spectrometers operating at 300 or 400 MHz (^{1}H NMR), and 100 MHz (^{13}C NMR), respectively. Chemical shifts (δ in ppm, coupling constants J in Hz) were referenced to residual solvent signals (^{1}H, ^{13}C). Assignments are based on homo- and heteronuclear shift correlation spectroscopy. Purity of bulk samples of the complexes has been established by NMR spectroscopy, and by elemental analysis, which were performed at the University of Bern Microanalytic Laboratory using a Thermo Scientific Flash 2000 CHNS-O elemental analyser. Residual solvent was confirmed by NMR spectroscopy and also by X–ray structure determinations. High-resolution mass spectrometry was carried out with a Thermo Scientific LTQ Orbitrap XL (ESI-TOF).

Electrochemistry. Electrochemical measurements were carried out using an EG&G Princeton Applied Research potentiostat model 273A typically at a 100 mV s^{-1} sweep rate employing a gastight three-electrode cell under an argon atmosphere. A Pt disk with a 3.80 mm^2 surface area was used as the working electrode and was polished before each measurement. The reference electrode was a Ag/AgCl electrode; the counter electrode was a Pt wire. Bu$_4$NPF$_6$ (0.1 M) in dry CH$_2$Cl$_2$ was used as a base electrolyte with analyte concentrations of approximately 10^{-3} M. The ferrocenium/ferrocene redox couple was used as an internal reference (E$_{1/2}$ = +0.46 V vs SCE in CH$_2$Cl$_2$).[36]

General procedure for amide formation (9a, 9b, and 13b). A solution of the acyl chloride (11 mmol) in THF (10 mL) was added dropwise to a solution of aminopyridine (0.940 g, 10 mmol) and NEt$_3$ (1.50 mL, 11 mmol) in THF (30 mL), which resulted in the formation of a white suspension. The reaction was refluxed for 48 h. After cooling to rt, the solids were removed by filtration and washed with THF (50 mL). The filtrates were combined and all volatiles were removed in vacuo to leave a white solid, which was purified by column chromatography (SiO$_2$; CH$_2$Cl$_2$/MeOH 95:5). All solvents were removed to yield the

corresponding amide as a white solid. Analytical data of these compounds are in agreement with those reported.[37,38]

I. General procedure for the formation of pyridinium salts (6a–c, 10a,b and 14a). *N*-(pyridin-4-yl)benzamide, **9a**,**b** or **13a** (2.0 mmol) was dissolved in MeCN (15 mL) in a pressure tube. The alkylating agent RI (R =^{i}Pr, ^{n}Bu or Oct, 3.0 mmol) was added and the reaction was stirred for 18 h at 80 °C. The solution was cooled to rt and concentrated to 5 mL. Et$_2$O (50 mL) was added affording compound as **6a–c, 10a**,**b** and **14a** a yellow solid, which was collected by filtration.

II. General procedure for synthesis of the pyridylidene amides (7a–c, 11a,b and 15a). A suspension of the pyridinium salt **6a–c, 10a,b** or **14a** (1.0 mmol) in CH$_2$Cl$_2$ (10 mL) was placed into a separating funnel. Aqueous NaOH (15 mL, 2M) was added. After vigorous mixing, the organic phase was collected. The aqueous layer was extracted with CH$_2$Cl$_2$ (3 x 15 mL), the combined organic layers were dried over anhydrous Na$_2$SO$_4$ and filtered. All volatiles were removed, thus giving free ligand **7a–c,** and **15a** as white-yellow solids, which were purified by recrystallization from pentane and **11a,b** as yellow oils.

III. General procedure for the synthesis of iridium complexes (8a–c, 12a,b and 16a). Compound **7a–c, 11a**,**b** or **15a** (0.4 mmol), NaOAc (33 mg, 0.4 mmol) and [Ir(Cp*)Cl$_2$]$_2$ (120 mg, 0.15 mmol) were dissolved in CH$_2$Cl$_2$ and stirred at rt for 18h. All volatiles were removed under reduced pressure and the crude solid was purified by column chromatography (SiO$_2$; CH$_2$Cl$_2$/MeOH 98:2), thus yielding **8a–c, 12a**.**b** and **16a** as orange solids.

Compound 6a

Compound **6a** was prepared according to the general procedure I from *N*-(pyridin-4-yl)benzamide, (396 mg, 2.0 mmol) and ^{i}PrI (294 μL, 3.0 mmol). Yield: 690 mg, 94%.

^{1}H NMR (300 MHz, d_6-DMSO): δ 11.54 (s, 1H, NH), 8.98 (d, $^{3}J_{HH}$ = 6.4 Hz, 2H, CH$_{pyr}$), 8.31 (d, $^{3}J_{HH}$ = 6.4 Hz, 2H, CH$_{pyr}$), 8.03 (d, 2H, $^{3}J_{HH}$ = 7.6, CH$_{Ph}$), 7.72 (t, 1H, $^{3}J_{HH}$ = 7.6 Hz, $^{4}J_{HH}$ = 1.3 Hz, CH$_{Ph}$), 7.63 (t, 2H, $^{3}J_{HH}$ = 7.6 Hz, CH$_{Ph}$), 4.88 (septet, 1H, $^{3}J_{HH}$ = 6.8 Hz, CHMe$_2$), 1.57 (d, 6H, $^{3}J_{HH}$ = 6.8 Hz, C–CH$_3$). ^{13}C{^{1}H} NMR (100 MHz, d_6-DMSO): δ 167.7 (CO), 152.4 (C$_{pyr}$), 143.3 (CH$_{pyr}$), 133.3 (CH$_{Ph}$), 132.9 (C$_{Ph}$), 128.8 (CH$_{Ph}$), 128.3 (CH$_{Ph}$), 115.9 (CH$_{pyr}$),

62.2 (CHMe$_2$), 22.3 (C–CH$_3$). HR-MS: m/z calculated for C$_{15}$H$_{17}$N$_2$O [M–I]$^+$ = 241.1341; found, 241.1329.

Compound 6b

Compound **6b** was prepared according to the general procedure I from *N*-(pyridin-4-yl)benzamide, (396 mg, 2.0 mmol) and *n*BuI (341 μL, 3.0 mmol). Yield: 728 mg, 95%.

^{1}H NMR (400 MHz, d_6-DMSO): δ 11.55 (s, 1H, NH), 8.88 (d, $^3J_{HH}$ = 7.3 Hz, 2H, CH_{pyr}), 8.31 (d, $^3J_{HH}$ = 7.3 Hz, 2H, CH_{pyr}), 8.11–7.96 (m, 2H, CH_{Ph}), 7.75–7.68 (m, 1H, CH_{Ph}), 7.64–7.60 (m, 2H, CH_{Ph}), 4.47 (t, $^3J_{HH}$ = 7.4 Hz, 2H, NCH_2), 1.86 (quint, $^3J_{HH}$ = 7.4 Hz, 2H, NCH$_2$CH_2), 1.29 (sext, $^3J_{HH}$ = 7.4 Hz, 2H, CH_2CH$_3$), 0.92 (t, $^3J_{HH}$ = 7.4 Hz, 3H, CH$_3$). ^{13}C{^{1}H} NMR (100 MHz, d_6-DMSO): δ 167.2 (CO), 152.0 (C$_{pyr}$), 145.0 (CH$_{pyr}$), 133.2 (CH$_{Ph}$), 132.9 (C$_{Ph}$), 128.8 (CH$_{Ph}$), 128.3 (CH$_{Ph}$), 115.7 (CH$_{pyr}$), 58.9 (NCH$_2$), 32.3 (NCH$_2$$CH_2$), 18.7 ($CH_2CH_3$), 13.3 (CH$_3$). HR-MS: m/z calculated for C$_{16}$H$_{19}$N$_2$O [M–I]$^+$ = 255.1492; found 255.1489. Elem. Anal. Calcd. for C$_{15}$H$_{19}$IN$_2$O: C, 50.28; H, 5.01; N, 7.33; Found: C, 50.31; H, 5.29; N, 7.53%.

Compound 6c

Compound **6c** was prepared according to the general procedure I from *N*-(pyridin-4-yl)benzamide, (396 mg, 2.0 mmol) and *n*OctI (541 μL, 3.0 mmol). Yield: 799 mg, 91%.

^{1}H NMR (400 MHz, d_6-DMSO): δ 11.55 (s, 1H, NH), 8.85 (d, $^3J_{HH}$ = 7.4 Hz, 2H, CH_{pyr}), 8.28 (d, $^3J_{HH}$ = 7.4 Hz, 2H, CH_{pyr}), 8.11–8.00 (m, 2H, CH_{Ph}), 7.78–7.67 (m, 1H, CH_{Ph}), 7.64–7.59 (m, 2H, CH_{Ph}), 4.44 (t, $^3J_{HH}$ = 7.2 Hz, 2H, NCH_2), 1.86 (quint, $^3J_{HH}$ = 7.2 Hz, 2H, NCH$_2$CH_2), 1.31–1.21 (m, 10H, CH$_2$), 0.86 (t, $^3J_{HH}$ = 7.0 Hz, 3H, CH$_3$). ^{13}C{^{1}H} NMR (100 MHz, d_6-DMSO): δ 167.4 (CO), 152.5 (C$_{pyr}$), 144.9 (CH$_{pyr}$), 133.1 (CH$_{Ph}$), 133.1 (C$_{Ph}$), 128.7 (CH$_{Ph}$), 128.3 (CH$_{Ph}$), 115.8 (CH$_{pyr}$), 59.1 (NCH$_2$), 31.1 (NCH$_2$$CH_2$), 30.3, 28.4, 28.3, 25.3, 22.0 (5 × CH$_2$), 13.9 (CH$_3$). HR-MS: m/z calculated for C$_{20}$H$_{27}$N$_2$O [M–I]$^+$ = 311.2118; found; 311.2111. Elem. Anal. Calcd. For C$_{20}$H$_{27}$IN$_2$O C, 54.80; H, 6.21; N, 6.39; Found: C, 54.83; H, 6.97; N, 6.37%.

Compound 7a

Compound **7a** was obtained as a white solid following the general procedure II from compound **6a** (368 mg, 1.0 mmol). Yield: 175 mg, 73%.

^{1}H NMR (300 MHz, d_6-DMSO): δ 8.13 (d, $^3J_{HH}$ = 6.0 Hz, 2H, CH_{pyr}), 8.12 (d, $^3J_{HH}$ = 7.3 Hz, 2H, CH_{Ph}), 7.47 (d, $^3J_{HH}$ = 6.0 Hz, 2H, CH_{pyr}), 7.42 (t, 1H, $^3J_{HH}$ = 7.3, CH$_{Ph}$), 7.38 (t, 2H, $^3J_{HH}$ = 7.3, CH$_{Ph}$ 4.45 (septet, 1H, $^3J_{HH}$ = 6.8, CHMe$_2$), 1.44 (d, 6H, $^3J_{HH}$ = 6.8, C–CH$_3$). ^{13}C{^{1}H}

NMR (100 MHz, d_6-DMSO): δ 173.9 (CO), 164.6 (C_{pyr}), 139.8 (C_{Ph}), 138.9 (CH_{pyr}), 130.1 (CH_{Ph}), 128.7 (CH_{Ph}), 127.6 (CH_{Ph}), 117.9 (CH_{pyr}), 58.7 ($CHMe_2$), 22.2 (C–CH_3). HRMS: m/z calculated for $C_{15}H_{17}N_2O$ $[M+H]^+$ = 241.1335; found, 241.1328. Elem. Anal. Calcd. for $C_{15}H_{16}N_2O$: C, 74.97; H, 6.71; N, 11.66; Found: C, 74.29; H, 6.22; N, 11.85%.

Compound 7b

Compound **7b** was obtained as a white solid following the general procedure II from compound **6b** (382 mg, 1.0 mmol). Yield: 219 mg, 84%.

^{1}H NMR (400 MHz, d_6-DMSO): δ 8.17–8.08 (m, 2H, CH_{Ph}), 8.02 (d, 2H, $^3J_{HH}$ = 7.4, CH_{pyr}), 7.46 (d, $^3J_{HH}$ = 7.4 Hz, 2H, CH_{pyr}), 7.43–7.34 (m, 3H, CH_{Ph}) 4.05 (t, $^3J_{HH}$ = 7.4 Hz, 2H, NCH_2), 1.73 (quint, $^3J_{HH}$ = 7.4 Hz, 2H, NCH_2CH_2), 1.26 (sext, $^3J_{HH}$ = 7.4 Hz, 2H CH_2CH_3), 0.90 (d, $^3J_{HH}$ = 7.4 Hz, 3H, CH_3). $^{13}C\{^1H\}$ NMR (100 MHz, d_6-DMSO): δ 173.8 (CO), 164.2 (C_{pyr}), 140.9 (CH_{pyr}), 139.7 (C_{Ph}), 130.1 (CH_{Ph}), 128.7 (CH_{Ph}), 127.5 (CH_{Ph}), 117.7 (CH_{pyr}), 56.2 (NCH_2), 32.3 (NCH_2CH_2), 18.8 (CH_2CH_3), 13.4 (CH_3). HR-MS: m/z calculated for $C_{16}H_{19}N_2O$ $[M+H]^+$ = 255.1492; found; 255.1485. Elem. Anal. Calcd. for $C_{16}H_{18}N_2O$: C, 75.56; H, 7.13; N, 11.01; Found: C, 75.34; H, 7.02; N, 11.01%.

Compound 7c

Compound **7c** was obtained as white solid following the general procedure II from compound **6c** (438 mg, 1.0 mmol). Yield: 239 mg, 77%.

^{1}H NMR (400 MHz, d_6-DMSO): δ 8.23–8.08 (m, 2H, CH_{Ph}), 8.02 (d, 2H, $^3J_{HH}$ = 7.4, CH_{pyr}), 7.45 (d, $^3J_{HH}$ = 7.4 Hz, 2H, CH_{pyr}), 7.43–7.34 (m, 3H, CH_{Ph}) 4.04 (t, $^3J_{HH}$ = 7.2 Hz, 2H, NCH_2), 1.74 (quint, $^3J_{HH}$ = 7.2 Hz, 2H, NCH_2CH_2), 1.32–1.18 (m, 10H, CH_2), 0.85 (d, $^3J_{HH}$ = 6.8 Hz, 3H, CH_3). $^{13}C\{^1H\}$ NMR (100 MHz, d_6-DMSO): δ 173.9 (CO), 164.3 (C_{pyr}), 140.9 (CH_{pyr}), 139.8 (C_{Ph}), 130.1 (CH_{Ph}), 128.7 (CH_{Ph}), 127.5 (CH_{Ph}), 117.7 (CH_{pyr}), 56.5 (NCH_2), 31.1 (NCH_2CH_2), 30.3, 28.5, 28.4, 25.5, 22.0 (5 × CH_2), 13.9 (CH_3). HR-MS: m/z calculated for $C_{15}H_{18}N_2O$ $[M+H]^+$ = 311.2118; found; 311.2114. Elem. Anal. Calcd. for $C_{16}H_{18}N_2O$: C, 77.38; H, 8.44; N, 9.02; Found: C, 76.96; H, 8.40; N, 9.14%.

Compound 8a

Compound **8a** was prepared according to the general procedure III from **7a** (96 mg, 0.40 mmol) to give an orange solid. Yield: 98 mg, 54%.

^{1}H NMR (500 MHz, $CDCl_3$): δ 8.54 (d, $^3J_{HH}$ = 6.9 Hz, 2H, CH_{pyr}), 7.69 (d, $^3J_{HH}$ = 7.4 Hz, 1H, CH_{Ph}), 7.67 (d, $^3J_{HH}$ = 6.9 Hz, 2H, CH_{pyr}), 7.57 (d, $^3J_{HH}$ = 7.4 Hz, H, CH_{Ph}) 7.21 (t, $^3J_{HH}$ = 7.4

Hz, 1H, CH$_{Ph}$), 6.93 (t, $^3J_{HH}$ = 7.4 Hz, 1H, CH$_{Ph}$), 4.27 (septett, $^3J_{HH}$ = 7.0 Hz, 1H, CHMe$_2$), 1.54 (s, 15H, Cp–CH$_3$), 1.43 (d, $^3J_{HH}$ = 6.3 Hz, CH–CH_3). ^{13}C{^{1}H} NMR (125 MHz, CDCl$_3$): δ 181.1 (CO), 162.4 (C$_{pyr}$), 159.4 (C$_{Ph}$–Ir), 140.9 (C$_{Ph}$), 137.4 (CH$_{pyr}$), 136.2 (CH$_{Ph}$), 132.3 (CH$_{Ph}$), 127.9 (CH$_{Ph}$), 122.1 (CH$_{Ph}$), 121.1 (CH$_{pyr}$), 87.3 (C$_{Cp}$), 60.0 (NCHMe$_2$), 23.0 (CH–CH_3), 9.2 (Cp–CH$_3$). HR-MS: m/z calculated for C$_{25}$H$_{30}$IrN$_2$O [M–Cl]$^+$ = 567.1988; found, 567.1976. Elem Anal. Calcd. for C$_{25}$H$_{30}$ClIrN$_2$O x 0.5 CH$_2$Cl$_2$: C, 47.51; H, 4.85; N, 4.35; Found C, 47.99; H, 4.76; N, 4.31.

Compound 8b

Compound **8b** was prepared according to the general procedure III from **7b** (102 mg, 0.40 mmol) to give an orange solid. Yield: 110 mg, 76%.

^{1}H NMR (400 MHz, CDCl$_3$): δ 8.31 (d, $^3J_{HH}$ = 7.0 Hz, 2H, CH$_{pyr}$), 7.72 (dd, $^3J_{HH}$ = 7.6 Hz, $^4J_{HH}$ = 1.1 Hz 1H, CH$_{Ph}$), 7.61–7.52 (m, 3H, CH$_{pyr}$ + CH$_{Ph}$), 7.22 (td, $^3J_{HH}$ = 7.3 Hz, $^4J_{HH}$ = 1.5 Hz, 1H, CH$_{Ph}$), 6.95 (td, $^3J_{HH}$ = 7.3 Hz, $^4J_{HH}$ = 1.1 Hz, 1H, CH$_{Ph}$), 3.81–3.52 (m, 2H, NCH$_2$), 1.51–1.41 (m, 2H, NCH$_2$CH_2), 1.46 (s, 15H, Cp–CH$_3$), 1.11–0.93 (m, 2H, CH_2CH$_3$), 0.75 (t, $^3J_{HH}$ = 7.3 Hz, 2H, CH$_2$CH_3). ^{13}C{^{1}H} NMR (100 MHz, CDCl$_3$): δ 183.3 (CO), 162.4 (C$_{pyr}$), 159.6 (C$_{Ph}$–Ir), 141.2 (C$_{Ph}$), 140.3 (CH$_{pyr}$), 136.3 (CH$_{Ph}$), 132.2 (CH$_{Ph}$), 127.8 (CH$_{Ph}$), 122.1 (CH$_{Ph}$), 121.2 (CH$_{pyr}$), 87.2 (C$_{Cp}$), 58.3 (NCH$_2$), 32.2 (NCH$_2$CH_2), 19.2 (CH_2CH$_3$), 13.5 (CH$_2$CH_3), 9.1 (Cp–CH$_3$). HR-MS: m/z calculated for C$_{26}$H$_{32}$IrN$_2$O [M–Cl]$^+$ = 581.2144; found, 581.2125. Elem Anal. Calcd. for C$_{26}$H$_{32}$ClIrN$_2$O: C, 50.68; H, 5.23; N, 4.55; Found: C, 50.12; H, 4.98; N, 4.53%.

Compound 8c

Compound **8c** was prepared according to the general procedure III from **7c** (124 mg, 0.40 mmol) to give an orange solid. Yield: 120 mg, 75%.

^{1}H NMR (400 MHz, CDCl$_3$): δ 8.30 (d, $^3J_{HH}$ = 7.1 Hz, 2H, CH$_{pyr}$), 7.71 (dd, $^3J_{HH}$ = 7.5 Hz, $^4J_{HH}$ = 1.0 Hz 1H, CH$_{Ph}$), 7.62–7.56 (m, 1H, CH$_{Ph}$), 7.57 (d, $^3J_{HH}$ = 7.1 Hz, 2H, CH$_{pyr}$), 7.21 (td, $^3J_{HH}$ = 7.3 Hz, $^4J_{HH}$ = 1.5 Hz, 1H, CH$_{Ph}$), 6.94 (td, $^3J_{HH}$ = 7.3 Hz, $^4J_{HH}$ = 1.3 Hz, 1H, CH$_{Ph}$), 3.72–3.53 (m, 2H, NCH$_2$), 1.45 (s, 15H, Cp–CH$_3$),1.44–1.39 (m, 2H, NCH$_2$CH_2), 1.30–1.21 (m, 2H, CH$_2$), 1.19–1.08 (m, 6H, CH$_2$), 0.96–0.86 (m, 2H, CH$_2$), 0.86 (t, $^3J_{HH}$ = 7.1 Hz, 3H, CH$_2$CH$_3$). ^{13}C{^{1}H} NMR (100 MHz, CDCl$_3$): δ 183.2 (CO), 162.5 (C$_{pyr}$), 159.6 (C$_{Ph}$–Ir), 141.2 (C$_{Ph}$), 140.4 (CH$_{pyr}$), 136.3 (CH$_{Ph}$), 132.2 (CH$_{Ph}$), 127.7 (CH$_{Ph}$), 122.1 (CH$_{Ph}$), 121.2 (CH$_{pyr}$), 87.2 (C$_{Cp}$), 58.6 (NCH$_2$), 31.7 (NCH$_2$CH_2), 31.2, 29.1, 28.9, 25.9, 22.7 (5 × CH$_2$), 14.2 (CH$_2$CH_3), 9.1 (Cp–CH$_3$). HR-MS: m/z calculated for C$_{30}$H$_{40}$IrN$_2$O [M–Cl]$^+$ = 637.2770; found, 637.2739.

Elem Anal. Calcd. for $C_{30}H_{40}ClIrN_2O \times 0.5 \, CH_2Cl_2$: C, 51.15; H, 5.43; N, 3.92; Found: C, 50.58; H, 5.43; N, 3.84%.

Compound 10a

Compound **10a** was prepared according to the general procedure I from **9a** (396 mg, 2.0 mmol) and MeI (187 µL, 3.0 mmol): Yield 251 mg, 39%.

^{1}H NMR (400 MHz, d_6-DMSO): δ 11.40 (s, 1H, NH), 8.95 (d, $^3J_{HH}$ = 6.3, Hz, 1H, CH_{pyr}), 8.58 (t, $^3J_{HH}$ = 8.1, $^4J_{HH}$ = 1.4 Hz, 1H, CH_{pyr}), 8.22 (dd, $^3J_{HH}$ = 8.1, $^4J_{HH}$ = 1.4 Hz, 1H, CH_{pyr}), 8.11–8.01 (m, 2H, CH_{Ph}), 7.89 (t, $^3J_{HH}$ = 6.3 Hz, 1H, CH_{pyr}), 7.75–7.68 (m, 1H, CH_{Ph}), 7.65–7.59 (m, 2H, CH_{Ph}), 4.29 (s, 3H, NCH_3). $^{13}C\{^1H\}$ NMR (100 MHz, d_6-DMSO): δ 166.6 (CO), 148.1 (C_{pyr}), 146.0 (CH_{pyr}), 145.6 (CH_{pyr}), 133.2 (CH_{Ph}), 132.5 (C_{Ph}), 128.7 (CH_{Ph}), 128.6 (CH_{Ph}), 124.1 (CH_{pyr}), 123.2 (CH_{pyr}), 44.3 (NCH_3). HR-MS: m/z calculated for $C_{13}H_{13}N_2O$ [M–I]$^+$ = 213.1022; found, 213.1025. Elem. Anal. Calcd. For for $C_{13}H_{13}IN_2O \times 0.5 \, H_2O$: C, 44.72; H, 4.04; N, 8.02; Found: C, 44.43; H, 3.90; N, 7.98%.

Compound 10b

Compound **10b** was prepared according to the general procedure I from **9b** (396 mg, 2.0 mmol) and MeI (187 µL, 3.0 mmol): Yield 646 mg, 95%.

^{1}H NMR (400 MHz, d_6-DMSO): δ 11.17 (s, 1H, NH), 9.52 (s, 1H, CH_{pyr}), 8.76 (d, $^3J_{HH}$ = 5.9, Hz 1H, CH_{pyr}), 8.65 (d, $^3J_{HH}$ = 8.8 Hz, 1H, CH_{pyr}), 8.14 (dd, $^3J_{HH}$ = 8.8, 5.9 Hz, 1H, CH_{pyr}), 8.05–7.99 (m, 2H, CH_{Ph}), 7.73–7.66 (m, 1H, CH_{Ph}), 7.64–7.57 (m, 2H, CH_{Ph}), 4.41 (s, 3H, NCH_3). $^{13}C\{^1H\}$ NMR (100 MHz, d_6-DMSO): δ 166.3 (CO), 140.3 (C_{pyr}), 139.0 (CH_{pyr}), 136.3 (CH_{pyr}), 134.6 (CH_{pyr}), 133.0 (C_{Ph}), 132.8 (CH_{Ph}), 128.5 (CH_{Ph}), 127.9 (CH_{Ph}), 127.8 (CH_{pyr}), 48.6 (NCH_3). HR-MS: m/z calculated for $C_{13}H_{13}N_2O$ [M–I]$^+$ = 213.1022; found, 213.1032.

Compound 11a

Compound **11a** was obtained as pale yellow oil following the general procedure II from compound **10a** (320 mg, 1.0 mmol). Yield: 174 mg, 82%.

^{1}H NMR (400 MHz, d_6-DMSO): δ 8.31 (d, $^3J_{HH}$ = 8.9, Hz, 1H, CH_{pyr}), 8.21–8.17 (m, 2H, CH_{Ph}), 8.17–8.13 (m, 1H, CH_{pyr}), 7.74 (ddd, $^3J_{HH}$ = 8.1, 6.7, $^4J_{HH}$ = 1.5 Hz 1H, CH_{pyr}), 7.49–7.36 (m, 3H, CH_{Ph}), 6.73 (td, $^3J_{HH}$ = 6.7, $^4J_{HH}$ = 1.5 Hz, 1H, CH_{pyr}), 3.87 (s, 3H, NCH_3). $^{13}C\{^1H\}$ NMR (100 MHz, d_6-DMSO): δ 172.0 (CO), 158.4 (C_{pyr}), 141.0 (CH_{pyr}), 140.1 (CH_{pyr}), 139.4 (C_{Ph}), 130.5 (CH_{Ph}), 128.8 (CH_{Ph}), 127.7 (CH_{Ph}), 119.2 (CH_{pyr}), 111.2 (CH_{pyr}), 41.0 (NCH_3). HR-MS: m/z calculated for $C_{13}H_{13}N_2O$ [M+H]$^+$ = 213.1022; found, 213.1022.

Compound 11b

Compound **11b** was obtained as pale yellow oil following the general procedure II from compound **10b** (320 mg, 1.0 mmol). Yield: 145 mg, 68%.

^{1}H NMR (400 MHz, d_6-DMSO): δ 9.22 (s, 1H, CH$_{pyr}$), 8.32 (d, $^3J_{HH}$ = 9.0 Hz, 1H, CH$_{pyr}$), 8.20–8.09 (m, 2H, CH$_{Ph}$), 8.02 (d, $^3J_{HH}$ = 5.8 Hz, 1H, CH$_{pyr}$), 7.66 (dd, $^3J_{HH}$ = 9.0, 5.8 Hz, 1H, CH$_{pyr}$), 7.30–7.26 (m, 3H, CH$_{Ph}$), 4.20 (s, 3H, NCH$_3$). ^{13}C{^{1}H} NMR (100 MHz, d_6-DMSO): δ 170.5 (CO), 153.8 (C$_{pyr}$), 141.2 (C$_{Ph}$), 138.6 (CH$_{pyr}$), 136.4 (CH$_{pyr}$), 131.6 (CH$_{pyr}$), 128.9 (CH$_{Ph}$), 128.2 (CH$_{Ph}$), 127.2 (CH$_{Ph}$), 126.3 (CH$_{pyr}$), 47.3 (NCH$_3$). HR-MS: m/z calculated for C$_{13}$H$_{13}$N$_2$O [M+H]$^+$ = 213.1022; found, 213.1030.

Compound 12a

Compound **12a** was prepared according to the general procedure III from **11a** (85 mg, 0.40 mmol) to give an orange solid. Yield: 124 mg, 72%.

^{1}H NMR (400 MHz, CD$_2$Cl$_2$): δ 8.74 (bs, 1H, CH$_{pyr}$), 8.08–7.94 (m, 2H, CH$_{pyr}$), 7.72 (d, $^3J_{HH}$ = 7.5 Hz, 1H, CH$_{Ph}$), 7.54 (dd, $^3J_{HH}$ =7.5, $^4J_{HH}$ = 1.6 Hz, 1H, CH$_{Ph}$), 7.25–7.15 (m, 1H, CH$_{pyr}$), 7.25–7.15 (m, 1H, CH$_{Ph}$), 6.96 (td, $^3J_{HH}$ = 7.3, $^4J_{HH}$ = 1.2 Hz, 1H, CH$_{Ph}$), 3.96 (s, 3H, NCH$_3$), 1.46 (s, 15H, Cp–CH$_3$). ^{13}C{^{1}H} NMR (100 MHz, CD$_2$Cl$_2$): δ 179.6 (CO), 162.2 (C$_{pyr}$), 158.6 (C$_{Ph}$–Ir), 142.8 (CH$_{pyr}$), 141.1 (CH$_{pyr}$), 140.4 (C$_{Ph}$), 136.3 (CH$_{Ph}$), 131.8 (CH$_{Ph}$), 129.1 (CH$_{pyr}$), 128.6 (CH$_{Ph}$), 121.1 (CH$_{Ph}$), 119.6 (CH$_{pyr}$), 87.5 (C$_{Cp}$), 44.9 (NCH$_3$), 9.4 (Cp–CH$_3$). HR-MS: m/z calculated for C$_{23}$H$_{26}$IrN$_2$O [M–Cl]$^+$ = 539.1669; found, 539.1665. Elem. Anal. Calcd. For C$_{23}$H$_{26}$ClIrN$_2$O: C, 48.12; H, 4.56; N, 4.88; Found: C, 47.37; H, 4.30; N, 4.69.

Compound 12b

Compound **12b** was prepared according to the general procedure III from **11b** (85 mg, 0.40 mmol) to give an orange solid. Yield: 117 mg, 68%.

^{1}H NMR (400 MHz, CD$_2$Cl$_2$): δ 9.65 (s, 1H, CH$_{pyr}$), 9.00 (d, $^3J_{HH}$ = 8.7 Hz, 1H, CH$_{pyr}$), 7.70 (d, $^3J_{HH}$ = 7.6 Hz, 1H, CH$_{Ph}$), 7.67 (d, $^3J_{HH}$ = 5.9 Hz, 1H, CH$_{pyr}$), 7.55–7.45 (m, 2H, CH$_{Ph}$ + CH$_{pyr}$), 7.17 (td, $^3J_{HH}$ = 7.6, $^4J_{HH}$ = 1.5 Hz, 1H, CH$_{Ph}$), 6.93 (t, $^3J_{HH}$ = 7.6 Hz, 1H, CH$_{Ph}$), 4.12 (s, 3H, NCH$_3$), 1.47 (s, 15H, Cp–CH$_3$). ^{13}C{^{1}H} NMR (100 MHz, CD$_2$Cl$_2$): δ 181.1 (CO), 158.7 (C$_{Ph}$–Ir), 152.9 (C$_{pyr}$), 141.8 (C$_{Ph}$), 141.6 (CH$_{pyr}$), 141.0 (CH$_{pyr}$), 136.3 (CH$_{Ph}$), 133.3 (CH$_{pyr}$), 131.6 (CH$_{Ph}$), 127.9 (CH$_{pyr}$), 126.9 (CH$_{Ph}$), 121.9 (CH$_{Ph}$), 87.3 (C$_{Cp}$), 48.8 (NCH$_3$), 9.4 (Cp–CH$_3$). HR-MS: m/z calculated for C$_{23}$H$_{26}$IrN$_2$O [M–Cl]$^+$ = 539.1669; found,

539.1684. Elem. Anal. Calcd. For $C_{23}H_{26}ClIrN_2O$ x 0.2 CH_2Cl_2: C, 47.14; H, 4.50; N, 4.74; Found: C, 46.96; H, 4.31; N, 4.57%.

Compound 14a

Compound **14a** was prepared according to the general procedure I from **13a** (576 mg, 2.0 mmol) and MeI (187 μL, 3.0 mmol): Yield 500 mg, 58%.

^{1}H NMR (300 MHz, CD_3CN): δ 10.32 (s, 1H, NH), 8.63 (dd, $^3J_{HH}$ = 6.4, $^4J_{HH}$ = 1.7 Hz, CH_{pyr} 1H, CH_{pyr}), 8.46 (td, $^3J_{HH}$ = 8.1, $^4J_{HH}$ = 1.7, 1H, CH_{pyr}), 8.26 (dd, $^3J_{HH}$ = 7.7, $^4J_{HH}$ = 1.4 Hz, 1H, CH_{pyr}), 7.77 (ddd, $^3J_{HH}$ = 8.1, 6.4, $^4J_{HH}$ = 1.4 Hz, 1H, CH_{pyr}), 7.42 (s, 2H, CH_{Ph}), 4.30 (s, 3H, NCH_3), 3.94 (s, 6H, OCH_3), 3.79 (s, 3H, OCH_3). $^{13}C\{^1H\}$ NMR (100 MHz, d_6-DMSO): δ 166.3 (CO), 153.9 (C_{Ph}), 148.8 (C_{pyr}), 146.9 (CH_{pyr}), 146.1 (CH_{pyr}), 142.6 (C_{Ph}), 127.5 (C_{Ph}), 125.9 (CH_{pyr}), 124.6 (CH_{pyr}), 106.8 (CH_{Ph}), 60.7 (OCH_3), 57.0 (OCH_3), 46.2 (NCH_3). Elem. Anal. Calcd. For $C_{16}H_{19}IN_2O_4$: C, 44.67; H, 4.45; N, 6.51; Found: C 44.29; H, 4.58; N, 6.30%.

Compound 15a

Compound **15a** was obtained as pale yellow solid following the general procedure II from compound **14a** (320 mg, 1.0 mmol). Yield: 241 mg, 80%

^{1}H NMR (400 MHz, d_6-DMSO): δ 8.26 (d, $^3J_{HH}$ = 8.7 Hz, 1H, CH_{pyr}), 8.15 (dd, $^3J_{HH}$ = 6.6, $^4J_{HH}$ = 1.8 Hz, 1H, CH_{pyr}), 7.73 (ddd, $^3J_{HH}$ = 8.7, 6.6, $^4J_{HH}$ = 1.8 Hz, 1H, CH_{pyr}), 7.51 (s, 2H, CH_{Ph}), 6.72 (td, $^3J_{HH}$ = 6.6, $^4J_{HH}$ = 1.8 Hz, 1H, CH_{pyr}), 3.87 (s, 3H, NCH_3), 3.83 (s, 6H, OCH_3), 3.71 (s, 3H, OCH_3). $^{13}C\{^1H\}$ NMR (100 MHz, d_6-DMSO): δ 171.4 (CO), 158.2 (C_{pyr}), 152.1 (C_{Ph}), 141.0 (CH_{pyr}), 140.0 (CH_{pyr}), 139.8 (C_{Ph}), 134.9 (C_{Ph}), 119.0 (CH_{pyr}), 111.0 (CH_{pyr}), 106.1 (CH_{Ph}), 60.0 (OCH_3), 55.7 (OCH_3), 41.0 (NCH_3). HR-MS: m/z calculated for $C_{16}H_{19}N_2O_4$ $[M+H]^+$ = 303.1339; found, 303.1338.

Compound 16a

Compound **16a** was prepared according to the general procedure III from **15a** (120 mg, 0.40 mmol) to give an orange solid. Yield: 165 mg, 69%.

^{1}H NMR (400 MHz, CD_2Cl_2): δ 8.92 (bs, 1H, CH_{pyr}), 8.01–7.90 (m, 2H, CH_{pyr}), 7.20 (td, $^3J_{HH}$ = 6.9, $^4J_{HH}$ = 1.5 Hz, 1H, CH_{pyr}), 7.08 (s, 1H, CH_{Ph}), 3.97 (s, 3H, NCH_3), 3.93 (s, 3H, OCH_3), 3.83 (s, 3H, OCH_3), 3.71 (s, 3H, OCH_3), 1.46 (s, 15H, $Cp–CH_3$). $^{13}C\{^1H\}$ NMR (100 MHz, d_6-DMSO): δ 178.8 (CO), 161.5 (C_{pyr}), 156.3 (C_{Ph}–Ir), 149.8 (C_{Ph}), 146.1 (C_{Ph}), 143.4 (C_{Ph}), 142.6 (CH_{pyr}), 140.5 (CH_{pyr}), 134.6 (C_{Ph}), 128.6 (CH_{pyr}), 119.5 (CH_{pyr}), 108.4 (CH_{Ph}), 87.5 (C_{Cp}), 61.5 (OCH_3), 60.9 (OCH_3), 56.1 (OCH_3), 44.7 (NCH_3), 9.5 ($Cp–CH_3$). HR-MS: m/z calculated for

$C_{26}H_{32}IrN_2O_4$ $[M–Cl]^+$ = 629.1991; found, 629.1974. Elem. Anal. Calcd. For $C_{26}H_{32}ClIrN_2O_4$: C, 47.02; H, 4.86; N, 4.22; Found: C, 46.94; H, 4.86; N, 4.13.

Dynamic Oxygen Evolution Measurements. For oxygen evolution measurements, a solution of the iridium complex (1 mL) was injected into a sealed 40 mL EPA vial containing 10 mL CAN solution (~ 0.4 M) buffered in 1M HNO_3. The generated oxygen lead to an increase in gas phase pressure, which was dynamically monitored *via* differential digital manometry as described previously.[8] End points of the reactions were verified by gas chromatography and corrected for nitrogen contamination.

DFT Calculations. All DFT calculations were performed with Gaussian 09 using B3LYP functional and LANL2DZ basis set. Default parameters and thresholds were used for gradient convergence. Geometry optimizations were carried out without additional constraints of solvent environment. The optimized geometries of the complexes were visualized with Avogadro.[39]

Crystal structure determinations. Suitable crystals of **8b**, **8c**, **12b** and **16a** were mounted in air at ambient conditions and measured on an Oxford Diffraction SuperNova area-detector diffractometer at T = 173(2) K using mirror optics monochromated Mo $K\alpha$ radiation (λ = 0.71073 Å) and Al filtered.[40] Data reduction was performed using the CrysAlisPro program.[41] The intensities were corrected for Lorentz and polarization effects, and an absorption correction based on the multi-scan method using SCALE3 ABSPACK in CrysAlisPro was applied. The structures were solved by direct methods using SHELXT,[42] and all non-hydrogen atoms were refined anisotropically. All H-atoms were placed in geometrically calculated positions and refined using a riding model with each H-atom assigned a fixed isotropic displacement parameter (1.2Ueq of its parent atom, 1.5Ueq for the methyl groups). Structures were refined on F^2 using full-matrix least-squares procedures. The weighting schemes were based on counting statistics and included a factor to downweight the intense reflections. All calculations were performed using the SHELXL-2014 program.[42]

The crystal of **8b** contains two independent molecules of the metal complex in the asymmetric unit and one co-crystallized CH_2Cl_2 molecule. The liberation of the butyl chain of one of the two independent molecules was found to be quite large (probably affected by some dynamic disorder that could not be modelled properly). A restraint on the most external C–C bond

distance was applied as well as a limitation of the anisotropic displacement parameter for the two C atoms involved. The crystal of **8c** contains two metal complex molecules and one co-crystallized dichloromethane molecule in the asymmetric unit. Part of one octyl group is disordered over two conformations. The co-crystallized dichloromethane molecule is disordered over two sites. The geometries of the disordered moieties were restrained to be equal. Its ADP's were restrained by the SHELXL SIMU and DELU instructions. The crystal **12b** contains two independent molecules of the complex in the asymmetric unit and co-crystallized CH_2Cl_2 (one molecule in general position, one disordered about an inversion center). The crystal possesses pseudo-translational elements that would produce a C-1 type structure (equivalent to a P-1 with halved volume). This would imply that the two complexes are equivalent but their conformation clearly differ, especially in the Cp* group. Moreover, the position of the clathrated solvent about the inversion center makes the double unit cell the best suggestion (as also proved by the accurate analysis of the weaker reflections). A structure solved in C-1 gave clearly worse refinement indices (R1 = 3.37%, instead of 2.18% of the P-1 solution) and larger atomic displacement parameters, especially for the Cp* atoms. Moreover, the pseudo C translation would be violated by half of the measured reflections. For compound **16a**, there are two solvent molecules in a crystal structure. Position of water molecule was refined without doubts, but the second one was assumed a CH_2Cl_2 molecule as it was used for crystallization. The molecule is highly disordered and no hydrogen atoms were assigned. Chlorine and carbon atoms were assigned according to the donor-acceptor adjacent of the molecule. Further details are given in Tables S2–S5. Crystallographic data for all four structures have been deposited with the Cambridge Crystallographic Data Centre (CCDC) as supplementary publication numbers 1585829 (**8b**), 1585830 (**8c**), 1585831 (**12b**), and 1585832 (**16a**).

References

[1] a) EIA, *2012 International Energy Outlook*, **2012**. b) J. T. Kiehl, K. E. Trenberth, *Bull. Am. Meteorol. Soc.* **1997**, *78*, 197–208.

[2] a) R.E. Blankenship, *Molecular Mechanisms of Photosynthesis.* Blackwell Science (Oxford), 2002; b) T. Gust, D. A. Moore, A. L. Moore, *Acc. Chem. Res.* **2009**, *42*, 1890–1898; c) S. Berardi, S. Drouet, L. Francas, C. Gimbert-Surinach, M. Guttentag, C. Richmond, T. Stoll, A. Llobet, *Chem. Soc. Rev.* **2014**, 43, 7501–7519; for a recent example, see: d) C. Liu, B. C. Colon, M. Ziesack, P. A. Silver, D. G. Nocera, *Science* **2016**, *352*, 1210–1213.

[3] a) N. D. McDaniel, S. Bernhard, *Dalton Trans.* **2010**, *39*, 10021–10030; b) S. Romain, L. Vigara, A. Llobet, *Acc. Chem. Res.* **2009**, *42*, 1944–1953.

[4] A. W. Rutherford, A.Boussac, *Science* **2004**, *303*, 1782–1784.

[5] a) K. N. Ferreira, T. M. Iversion, K. Maghlaoui, J. Barber, S.Iwata, *Science* **2004**, *303*, 1831–1838; b) J. P. McEvoy, G. W. Brudvig, *Chem. Rev.* **2006**, *106*, 4455–4484; c) Y. Umena, K. Kawakami, Y.-R. Shen, N. Kamiya, *Nature* **2011**, *473*, 55–60.

[6] For pioneering work using bimetallic catalysts: a) S. W. Gersten, J. G. Samuels, T. J. Meyer, *J. Am. Chem. Soc.* **1982**, *104*, 3855–3864; b) J. A. Gilbert, D. S. Eggleston, W. R. Murphy, D. A. Geselowitz, S. W. Gersten, D. J. Hodgson, T. J. Meyer, *J. Am. Chem. Soc.* **1985**, *107*, 3855–3864; c) C. Sens, I. Romero, M. Rodríguez, A. Llobet, T. Parella, J. Benet-Buchholz, *J. Am. Chem. Soc.* **2004**, *126*, 7798–7799; d) J. Limburg, J. S. Vrettos, H. Chen, J. C. de Paula, R. H. Crabtree, G. W. Brudvig, *J. Am. Chem. Soc.* **2001**, *123*, 423–430.

[7] For pioneering work using tetrametallic catalytic systems, see: a) A. Sartorel, M. Carraro, G. Scorrano, R. De Zorzi, S. Ceremia, N. D. McDaniel, S. Bernhard, M. Bonchio, *J. Am. Chem. Soc.* **2005**, *127*, 12802–12803; b) A. Sartorel, P. Miró, E. Salvadori, S. Romain, M. Carraro, G. Scorrano, M. Di Valentin, A. Llobet, C. Bo, M.Bonchio, *J. Am. Chem. Soc.* **2009**, *131*, 16051–16053; c) Y. V. Geletii, B. Botar, P. Kögerler, D. A. Hillesheim, D. G. Musaev, C. L. Hill, *Angew. Chem. Int. Ed.* **2008**, *47*, 3896–3899; d) F. Song, R. More, M. Schilling, G. Smolentsev, N. Azzaroli, T. Fox, S. Luber, G. R. Patzke, *J. Am. Chem. Soc.* **2017**, *139*, 14198–14208.

[8] N. D. McDaniel, F. J. Coughlin, L. L. Tinker, S. Bernhard, *J. Am. Chem. Soc.* **2008**, *130*, 210–217.

[9] a) J. J. Concepcion, J. W. Jurss, J. L. Templeton, T. J. Meyer, *J. Am. Chem. Soc.* **2008**, *130*, 16462–16463; b) H.-W. Tseng, R. Zong, J. T. Muckerman, R. Thummel, *Inorg. Chem.* **2008**, *47*, 11763–11773; c) D. J. Wasylenko, C. Ganesamoorthy, M. A. Henderson, B. D. Koivisto, H. D. Osthoff, C. P. Berlinguette, *J. Am. Chem. Soc.* **2010**, *132*, 16094–16106; d) S. Roeser, P. Farras, F. Bozoglian, M. Martinez-Belmonte, J. Benet-Buchholz, A. Llobet, *ChemSusChem* **2011**, *4*, 197–207.

[10] For pioneering work with Mn: a) R. Brimblecombe, G. F. Swiegers, G. C. Dismukes, L. Spiccia, *Angew. Chem.* **2008**, *120*, 7445–7448; b) G. C. Dismukes R. Brimblecombe, G. A. N. Felton, R. S. Pryadun, J: E. Sheats, L. Spiccia, G. F. Swiegers, *Acc. Chem. Res.* **2009**, *42*, 1935–1943; with Fe: c) W. C. Ellis, N. D. McDaniel, S. Bernhard, T. J. Collins, *J. Am. Chem. Soc.* **2010**, *132*, 10990–10991; d) J. Lloret Fillol, Z. Codola, I. Garcia-Bosch, L. Gomez, J. Jose Pla, M. Costas, *Nature Chem.* **2011**, *3*, 807–813; with Cu: e) S. M. Barnett, K. I. Goldberg, J. M. Mayer, *Nature Chem.* **2012**, *4*, 498–502. Catalysts based on Co or Ni are generally, heterogeneous, see: f) M. W. Kanan, D. G. Nocera, *Science* **2008**, *321*, 1072–1075; with Ni: g) M. Dince, Y. Surendranath, D. G. Nocera, *Proc. Nat. Acad. Sciene USA* **2010**, *107*, 10337–10341.

[11] a) J. A. Woods, S. Bernhard, M. Albrecht, in *Molecular Water Oxidation* (Ed. A. Llobet, ed.), Wiley-VCH (Weinheim), **2013**, 113–133; b) M. D. Kärkäs, O. Verho, E. V. Johnston, B. Åkermark, *Chem. Rev.* **2014**, *114*, 11863–12001; c) J. D. Blakemore, R. H. Crabtree, G. W. Brudvig, *Chem. Rev.* **2015**, *115*, 12974–13005; d) I. Corbucci, A. Macchioni, M. Albrecht in *Iridium(III) in Optoelectronic and Photonics Applications* (Ed. E. Zysman-Colman), Wiley-VCH (Weinheim), **2017**, 617–654.

[12] For ruthenium complexes with exceptionally high activity, see: a) L. Duan, F. Bozoglian, S. Mandal, B. Stewart, T. Privalov, A. Llobet, L. Sun, *Nature Chem.* **2012**, *4*, 418–423; b) R. Matheu, M. Z. Ertem, J. Benet-Buchholz, E. Coronado, V. S. Batista, X. Sala, A. Llobet, *J. Am. Chem. Soc.* **2015**, *137*, 10786–10795.

[13] J. F. Hull, D. Balcells, J. D. Blakemore, C. D. Incarvito, O. Eisenstein, G. W. Brudvig, R. H. Crabtree, *J. Am. Chem. Soc.* **2009**, *131*, 8730–8731.

[14] a) A. Savini, P. Belanzoni, G. Bellachioma, C. Zuccaccia, D. Zuccaccia, A. Macchioni, *Green Chem.* **2011**, *13*, 3360–3374; b) C. Zuccaccia, G. Bellachioma, O. Bortolini, A. Bucci, A. Savini, A. Macchioni, *Chem. Eur. J.* **2014**, *20*, 3446–3456.

[15] a) R. Lalrempuia, N. D. McDaniel, H. Müller-Bunz, S. Bernhard, M.Albrecht, *J. Am. Chem. Soc.* **2010**, *49*, 9765–9768; b) J. A. Woods, R. Lalrempuia, A. Petronilho, N. D. McDaniel, H. Müller-Bunz, M. Albrecht, S. Bernhard, *Energy Environ. Sci.* **2014**, *7*, 2316–2328; c) A. Petronilho, J. A. Woods, H. Mueller-Bunz, S. Bernhard, M. Albrecht, *Chem. Eur. J.* **2014**, *20*, 15775–15784; d) B. Mahanti, G. Gonzalez Miera, E. Martinez-Castro, M. Bedin, B. Martin-Matute, S. Ott, A. Thapper, *ChemSusChem* **2017**, *10*, 4616–4623.

[16] For examples of other efficient chelating systems, see: a) A. Bucci, A. Savini, L. Rocchigiani, C. Zuccaccia, S. Rizzato, A. Albinati, A. Llobet, A. Macchioni, *Organometallics* **2012**, *31*, 8071–8074; b) H. Junge, N. Marquet, A. Kammer, S. Denurra, M. Bauer, S. Wohlrab, F. Gärtner, M.-M. Pohl, A. Spannenberg, S. Gladiali, M. Beller, *Chem. Eur. J.* **2012**, *18*, 12749–12758; c) J. DePasquale, I. Nieto, L. E. Reuther, C. J. Herbst-Gervasoni, J. J. Paul, V. Mochalin, M. Zeller, C. M. Thomas, A. W. Addison, E. T. Papish, *Inorg. Chem.* **2013**, *52*, 9175–9183; d) A. Levandowska-Andralojc, D. E. Polyansky, C.-H. Wang, W.-H. Wang, Y. Himeda, E. Fujita, *Phys. Chem. Chem. Phys.* **2014**, *16*, 11976–11987; d) A. Bucci, G. Menendez Rodriguez, G. Bellachioma, C. Zuccaccia, A. Poater, L. Cavallo, A. Macchioni, *ACS Catal.* **2016**, *6*, 4559–4563; e) T. K. Michaelos, D. Y. Shopov, S. Bhushan Sinha, L. S. Sharninghausen, K. J. Fisher, H. M. C. Lant, R. H. Crabtree, G. W. Brudvig, *Acc. Chem. Res.* **2017**, *50*, 952–989.

[17] a) M. E. Doster, S. A. Johnson, *Angew. Chem. Int. Ed.* **2009**, *48*, 2185–2187; b) Q. Shi, R. J. Thatcher, J. Slattery, P. S. Sauari, A. C. Whitwood, P. C. McGowan, R. E. Douthwaite, *Chem. Eur. J.* **2009**, *15*, 11346–11360; c) P. D. W. Boyd, L. J. Wright, M. N. Zafar, *Inorg. Chem.* **2011**, *50*, 10522–10524; d) K. F. Donnelly, C. Segarra, L.-X. Shao, R. Suen, H. Müller-Bunz, M. Albrecht, *Organometallics* **2015**, *34*, 4076–4084.

[18] M. Navarro, M. Li, H. Müller-Bunz, S. Bernhard, M. Albrecht, *Chem. Eur. J.* **2016**, *22*, 6740–6745.

[19] M. Navarro, C. A. Smith, M. Albrecht, *Inorg. Chem.* **2017**, *56*, 11688–11701.

[20] I. Corbucci, A. Petronilho, H. Müller-Bunz, L. Rocchigiani, M. Albrecht, A. Macchioni, *ACS Catal.* **2015**, *5*, 2714–2718.

[21] A. Abbotto, S. Bradamante, G. A. Pagani, *J. Org. Chem.* **2001**, *66*, 8883–8892.

[22] a) D. L. Davies, S. M. A. Donald, S. A. Macgregor, *J. Am. Chem. Soc.* **2005**, *127*, 13754–13755; b) D. L. Davies, S. M. A. Donald, O. Al-Duaij, J. Fawcett, C. Little, S. A. Macgregor, *Organometallics* **2006**, *25*, 5976–5978; c) M. Albrecht. *Chem. Rev.* **2010**, *110*, 576–623.

[23] V. Leigh, D. D. Carleton, J. Olguin, H. Mueller-Bunz, L. J. Wright, M. Albrecht, *Inorg. Chem.* **2014**, *53*, 8054–8060.

[24] R. J. Thatcher, D. G. Johnson, J. M. Slattery, R. E. Douthwaite, *Chem. Eur. J.* **2012**, *18*, 4329–4336.

[25] M. Navarro, M. Li, S. Bernhard, M. Albrecht, *Dalton Trans.* **2018**, *47*, 659–662.

[26] T. van Dijk, S. Burck, M. K. Rong, A. J. Rosenthal, M. Nieger, J. C. Slootweg, K. Lammertsma, *Angew. Chem. Int. Ed.* **2014**, *53*, 9068–9071.

[27] A. Zweig, W. G. Hodgson, W. H. Jura, *J. Am. Chem. Soc.* **1964**, *86*, 4124–4129.

[28] For highly active iridium complexes, see: a) A. Bucci, A. Savini, L. Rocchigiani, C. Zuccaccia, S. Rizzato, A. Albinati, A. Llobet, A. Macchioni, *Organometallics* **2012**, *31*, 8071–8074; b) J. DePasquale, I. Nieto, L. E. Reuther, C. J. Herbst-Gervasoni, J. J. Paul, V. Mochalin, M. Zeller, C. M. Thomas, A. W. Addison, E. T. Papish, *Inorg. Chem.* **2013**, *52*, 9175–9183; c) A. Lewandowska-Andralojc, D. E. Polyansky, C.-H. Wang, W. H. Y. Himeda, E. Fujita, *Phys. Chem. Chem. Phys.* **2014**, *16*, 11976–11987; G. Menendez Rodriguez, A. Bucci, R. Hutchinson, G. Bellachioma, C. Zuccaccia, S. Giovagnoli, H. Idriss, A. Macchioni, *ACS Energy Lett.* **2017**, *2*, 105–110.

[29] This contrasts with ruthenium complexes, where the first oxidation state correlates well with catalytic rates, see for example: L. Bernet, R. Lalrempuia, W. Ghattas, H. Mueller-Bunz, L. Vigara, A. Llobet, M. Albrecht, *Chem. Commun.* **2011**, *47*, 8058–8060.

[30] One of such effects might be a possible reorganization of water molecules close to the metal coordination sphere due to the hydrophobic environment imparted by the hydrophobic alkyl chains. Also, the aliphatic chain may support the formation and stabilization of the critical oxo-species when it is located in a position close to the catalytically active site. The long chain aliphatic substituents in the PYA systems **8a–c**

are positioned far from the metal center and hence exert little influence on the active site, while the aliphatic chain on the triazolylidene complexes is adjacent to the metal-bound carbon and therefore affects the second coordination sphere more pronouncedly.

[31] For an example with Ru, see: J. J. Concepción, M.-K. Tsai, J. T. Muckerman, T. J. Meyer, *J. Am. Chem. Soc.* **2010**, *132*, 1545–1557.

[32] a) C. J. Gagliardi, A. K. Vannucci, J. J. Concepción, Z. Chen, T. J. Meyer, *Energy Environ. Sci.* **2012**, *5*, 7704–7717; b) T. J. Meyer, M. H. V. Huynh, H. H. Thorp, *Angew. Chem. Int. Ed.* **2007**, *46*, 5284–5304.

[33] The small difference between complexes **12b** and **16b** suggests that the mesoionic character of the PYA ligand mitigates the effect of MeO substituents at the phenyl ligand and therefore, electronic modulation does not show much effect.

[34] All calculations were performed on the unoxidized Ir(III) catalyst. It is noteworthy that the deprotonation of the water ligand and the metal oxidation required for driving water oxidation will likely decrease the metal–ligand distance, which will further increase the crowding of the ligand sphere around the aquo/hydroxyl ligand.

[35] R. G. Ball, W. A. G. Graham, D. M. Heinekey, J. K. Hoyono, A. D. McMaster, B. M. Mattson, S. T. Michel, *Inorg. Chem.* **1990**, *29*, 2023–2025.

[36] N. G. Connelly, W. E. Geiger, *Chem. Rev.* **1996**, *96*, 877–910.

[37] H.-A. Seo, Y.-H. Cho, T.-S. Lee, C.-H. Cheon, *J. Org. Chem.* **2015**, *80*, 11993–11998.

[38] O. P. S. Satel, D. Anand, R. K. Maurya, P. P. Yadav, *Green. Chem.* **2015**, *17*, 3728–3732.

[39] M. D. Hanwell, D. E. Curtis, D. C. Lonie, T. Vandermeersch, E. Zurek, G. R. Hutchison, *J. Cheminformatics* **2012**, *4*, 17.

[40] P. Macchi, H. B. Bürgi, A. S. Chimpri, J. Hauser, Z. Gal, *J. Appl. Cryst*, **2011**, *44*, 763–771.

[41] Oxford Diffraction (2010). *CrysAlisPro* (Version 1.171.34.44). Oxford Diffraction Ltd., Yarnton, Oxfordshire, UK.

[42] G. M. Sheldrick, *Acta Cryst.* **2015**, *A71*, 3–8.
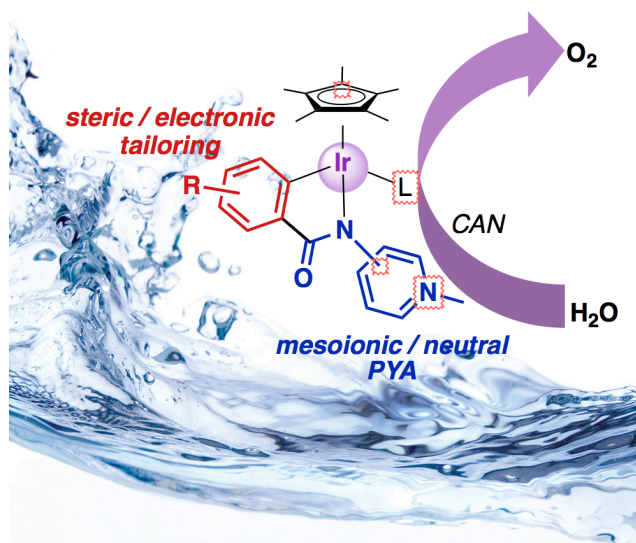
Pyridylidene-amide (PYA) ligands offer a versatile platform for synthetic modification and for tailoring catalytic activity, both by modulating the aryl substituent as well as by modifying the position of the pyridinium site from weakly donating to mesoionic PYA systems, and sterically congested 2-pyridylidene isomer, with profound impact on the catalytic activity of the iridium center in water oxidation.